Investigation of the Microstructure of Adiabatic Shear Bands in Pure Copper Under High Strain-Rate Deformation

By

Faranak Yazdani

A thesis
submitted to the faculty of graduate studies
in partial fulfillment of the
requirement for the degree of

MASTER OF SCIENCE

Department of Mechanical and Manufacturing Engineering
University of Manitoba
Winnipeg, Manitoba

Investigation of the Microstructure of Adiabatic Shear Bands in Pure Copper Under High Strain-Rate Deformation

BY

Faranak Yazdani

A Thesis/Practicum submitted to the Faculty of Graduate Studies of The University of Manitoba in partial fulfillment of the requirement of the degree

Of

MASTER OF SCIENCE

ABSTRACT

The properties of wide range of pure metals and alloys change during applications involving high speed rate of deformation due to the thermo-mechanical instability, which leads to strain localization and occurrence of adiabatic shear bands in materials. Therefore, it is of great importance to understand the way material properties, microstructural evolution, loading rates, and stress states affect formation of these bands. Adiabatic shear bands are preferred sites for failure initiation in material as they are usually harder and more brittle than the surrounding matrix; therefore, upon the formation of the ASB, the material is considered to have undergone failure for all intents and purposes.

Since most of the previous investigations concerning high strain rate testing have involved vastly around strong and tough materials such as steels, one question that always arises during this type of experiments is whether weaker and more ductile materials such as copper would behave the same way and form adiabatic shear bands. Therefore, in this thesis, the plastic deformation behavior of polycrystalline copper with purity of 99.94% is investigated at high strain rate using a Torsional Split Hopkinson bar. The key objective of this research is to confirm the occurrence of ASBs in copper and analyze the influence of the applied torque on the formation of these bands by testing the specimens at different twist angles ranging from 6° to 9°. Further analysis is done to determine the mechanisms of ABS formation as well as the relationship between material parameters and material deformation.

Microstructural examination of tested samples is performed by Scanning Electron Microscopy. All samples displayed an immensely deformed, highly localized region of deformation. These regions are considered to be the deformed type of adiabatic shear bands as there are two types of ASB, which will be described later.

The results in this study, which is a contribution to the field, show the strong influence of strain rate on the deformation of copper. High strain rates of up to 1361 s^{-1} are obtainable using Torsional Split Hopkinson bar to investigate the specimens. The average critical strain and time for strain localization are determined to lie between 0.30 – 0.58 and 163 – 178 μs respectively. The rate dependency of flow stress and strain are clearly observed from the results and how these properties increase with increase in applied strain rate. The mechanism of this increment and other related changes in certain properties of copper following the change in strain rate are described and discussed. Also due to the appearance of the large extended plastic deformation in tested copper samples, the more complex aspects of ASB formation mechanisms in copper than just the dislocation pile-up release that was found by Wright *et al.* are presented and discussed.

DEDICATION

I would like to dedicate this work to my father, my mother and my sister for their endless support throughout every single aspect of my life as well as to my uncle (Nariman Sepehri) and my aunt (Christine Wu), for their constant encouragement and occasional push which initiated the final effort in this thesis – without them I would not be standing where I am right now in my life.

ACKNOWLEDGEMENT

Patience was one of the most important requirements in order for this work to final come to end. However, there are great many people who contributed to a successful completion of this work. I would like to acknowledge my supervisor, Dr. M. Nabil Bassim for his encouragement and guidance through the completion of this work, which is greatly appreciated. The assistance of Dr. A. Odeshi in the experimental work of this study and taking the time to review the final draft of this work is greatly valued and highly appreciated.

There are many other people who played important role and deserve my appreciation during completion of this work. To those ones, who helped me through the rough time and gave me the permission to use their laboratory: Dr. Richards, Dr. Chaturvedi and Dr. Ojo. To all technicians who shared their excellent knowledge and experience with me; John Van Dorp, Don Mardis and Dan McCooeye. They have become great friends and their helps will always be remembered and respected. Lastly, lots of thanks to Dr. Ojo and Dr. Rattanawangcharoen for being my second examiners and giving me their time. I hope that I have not forgotten you and if I did, it is due to my own unawareness and not a lack of gratitude.

TABLE OF CONTENTS

LIST OF FIGURES

LIST OF TABLES

CHAPTER ONE: INTRODUCTION

The mechanisms of plastic deformation of metals and alloys are different under three different strain rates: quasi-static loading, low strain rates and high strain rates. In case of quasi-static loading and low strain rates, plastic deformation is governed by slip and twinning mechanisms. This type of deformation is usually uniform across the material, unlike plastic deformation at high strain rate, which is usually localized along narrow bands called adiabatic shear bands. This strain localization is usually caused by adiabatic heating in which heat is generated during deformation and leads to a local rise in temperature. It is due to this strain localization in the material that most sudden and unexpected failure happens during deformation at high strain rates.

Two types of adiabatic shear bands have been identified in the literature: deformed bands and white-etching bands (also known as transformed bands). The deformed shear band is a region of intense plastic deformation that most often occurs at a very first stage of shear deformation. This band has similar appearance to the bulk material and consists of highly distorted and elongated grains parallel to the direction of applied shear stress. They are commonly formed in low density materials such as copper and aluminum alloys. On the other hand, the white-etching shear band appears as white band whose microstructure consists of very fine sub-grains, which has very different appearance than the surrounding bulk material. It is obvious from the name that this band appears as a white band. This white nature of ASB plus a review of microstructure and properties of both types of ASBs will be enumerated in the literature review.

The presence of adiabatic shear bands will cause instability in the microstructure of material, which can be regarded as beginning of failure even if actual fracture and fragmentation does not occur and is therefore not desirable in structural parts. So far, most of the previous investigations on adiabatic shear bands since 1944 were mostly focused on its initiation and propagation and less on mechanisms of the formation of these bands. It seems that the mechanistic aspect and microstructural evaluation of adiabatic shear bands in materials such as steel are well defined and known; whereas in the case of copper, this information is vague and hardly recognized, and there are still some contradictions between some of the research studies done in the past. Therefore, the present work is aimed to confirm the formation of ASB in copper and investigate the different mechanisms that may contribute to the initiation and formation of these bands. Thus, first a review of previous work on initiation, propagation and properties of adiabatic shear bands in general is presented and the remaining chapters are dedicated specifically on copper. Then, in order to achieve the set research objective, thin-walled tube samples machined from commercially annealed, polycrystalline, 99.94% purity copper were subjected to rapid shear deformation by using a Torsional Split Hopkinson bar. The effects of certain parameters such as strain rate, thermal conductivity, rate of strain hardening, grain size and orientation and etc, on formation of adiabatic shear bands were considered in the present research. Scanning Electron Microscopy (SEM) is used to examine the detailed microstructural evolution involved in adiabatic shear bands formation in copper samples due to its higher resolution and depth of field compared to Optical Microscopy.

CHAPTER TWO: LITERATURE REVIEW

2.1 Adiabatic Shear Bands

Adiabatic shear bands (ASBs) are narrow bands of intense plastic shear strain in materials that are subjected to large strains at high strain rates (or equivalently for short period of times). During this high strain rate deformation, adiabatic heating usually occurs which would cause a local rise in temperature due to the heat generated in a region that is retained and not conducted away. If the strength loss due to this thermal softening becomes greater than the increase in strength due to strain hardening, the plastic deformation becomes unstable, resulting in an extreme localization of deformation along narrow bands called adiabatic shear bands. The phenomenon of adiabatic heating leading to strain localization and formation of shear bands during high strain-rate deformation was first described by Zener and Hollomon in 1944 [1, 2, 3]. Since then, numerous investigations have been carried out to understand the most unusual and unique features of adiabatic shear bands in term of mechanical, thermodynamic and metallurgical behavior.

Based on some theoretical and experimental evidence, the properties of a wide range of pure metals and alloys change at a strain rate around 10^3-10^5 s^{-1} due to a transition in the conditions of dislocation motion, which may lead to the formation of ASBs. Therefore, understanding the way material properties, microstructural evolution, loading rates, and stress states affect ASB formation is of considerable interest in applications that involve high strain rate deformation such as armour penetration, explosion fragmentation, dynamic blanking and cropping, high-speed machining and forming, ballistic impact, impact erosion and surface rubbing and so on. Zener and

Hollomon observed the effects of localized shear deformation in punching [3, 4]. While Wright showed that strain rate is sufficiently high enough to promote adiabatic heating and strain localization during high speed machining operations [1, 5].

2.1.1 Plastic Behavior of Materials at High Strain Rate

Based on results of several years of study by different researchers including Marchand and Duffy (1988) [6], the plastic deformation under high strain-rate appears to follow a three stage process (Fig. 2.1). The first stage, which starts immediately after yielding, is known as homogeneous strain state. Following the first stage is a general inhomogeneous strain state. It is at this intermediate stage that strain hardening and thermal softening compete with each other and strain begins to concentrate in a broad band that encircles the specimen. The localization of strain to a fine shear band happens at the final stage, which sometimes can be followed by failure similar to the one shown in Fig. 2.2 [7]. The different mechanisms of failure will be discussed in more detail.

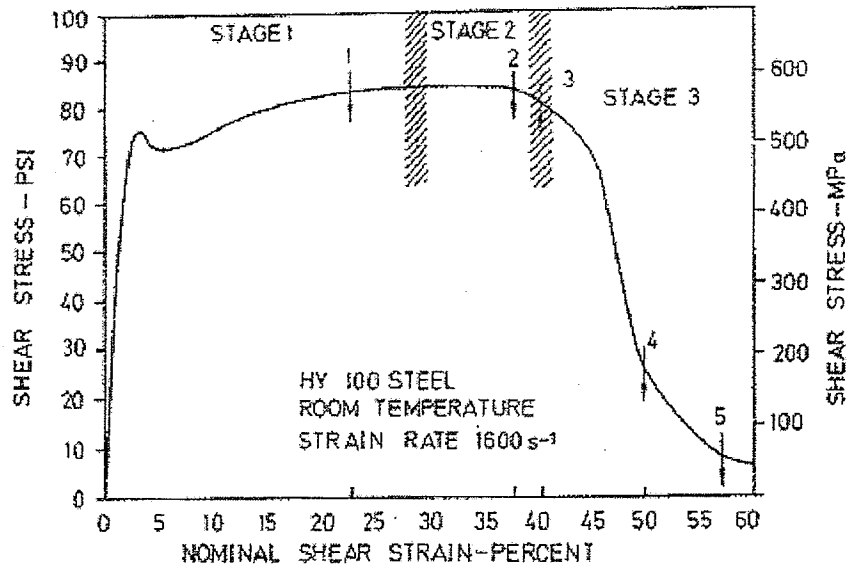

Fig. 2.1: Dynamic Stress-Strain Curve showing three stages of deformation at high strain rate [4]

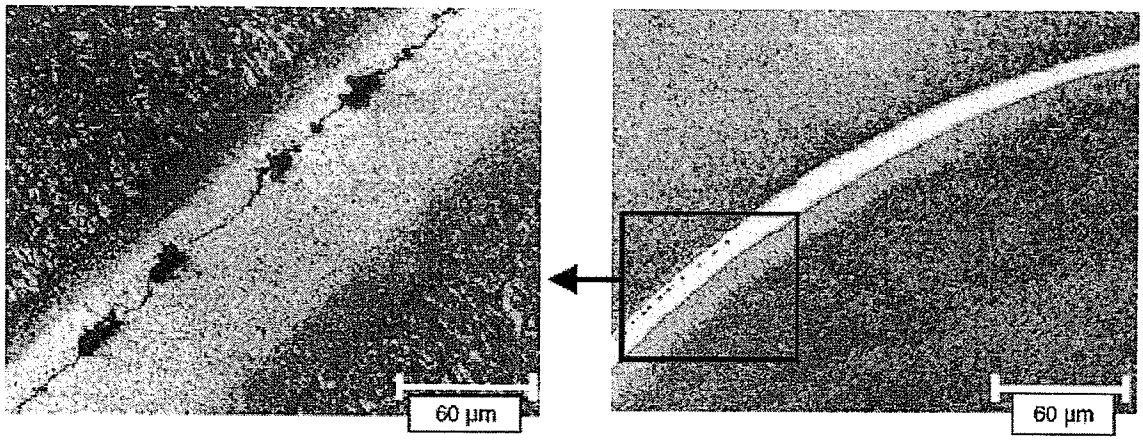

Fig. 2.2: Void formation preceding crack nucleation and propagation in the adiabatic shear band [7]

Fig. 2.3 shows typical responses of a work-hardening material during a torsion experiment [2]. Basically, there are two effects involved during plastic deformation: thermal softening due to the conversion of part of the deformation energy into heat energy and strain hardening due to dislocation multiplication. The isothermal line (dash line) in Fig. 2.3 represents the deformation at low strain rate, in which strain hardening dominates and the material continuously become hardened as strain increases. The solid line indicates the plastic deformation at high strain rate. At the beginning of the high strain rate deformation, work hardening controls the deformation process until the flow stress reaches maximum at $\gamma_{\text{max stress}}$. Beyond the maximum flow stress, the thermal softening dominates the process and the flow stress decreases with increasing strain. This thermal softening may continue indefinitely if a material is perfect with uniform distribution of stress, strain and temperature. However, most materials have non uniformities that can lead to stress collapse, strain localization and formation of adiabatic shear bands [1, 2].

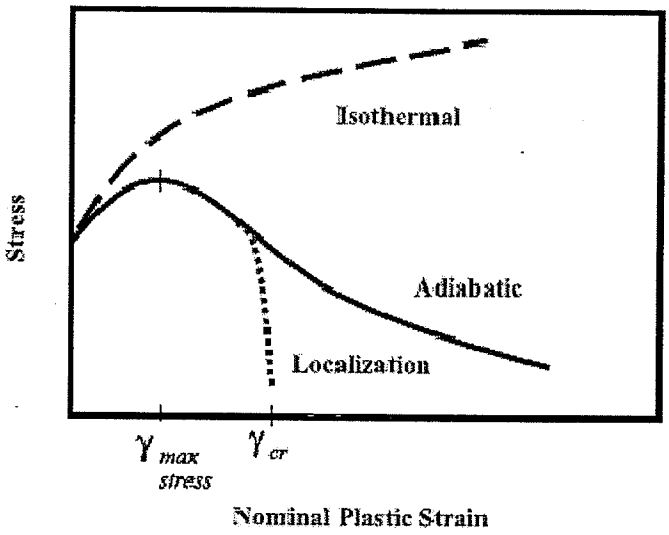

Fig. 2.3: Shear stress versus nominal shear strain for a typical work-hardening material during a torsion experiment [2]

2.1.2 Characteristic Aspects of Adiabatic Shear Bands

Generally, the mechanical behavior of most materials is found to be dependent on the high local value of the shear strain, shear strain rate and temperature within an adiabatic shear band. The local shear strains within shear bands commonly range between 5 to 100 [4, 8, 9] and the local strain rate can be as high as 10^7 s^{-1}. During high strain rate plastic deformation, the heat is generated inside the material that can increase the local temperature up to several hundred degrees and this can be measured directly as it was shown by Marchand and Duffy, 1988 [6] and others [4]. It is also very important to determine the fraction of the work which goes to increasing the temperature of the material, due to the fact that flow stress for some materials are temperature dependent and continuous rise of temperature during deformation can result in simultaneous lowering of the flow stress. The study by Kapoor and Nemat-Nasser (1998) [10] on several materials including OFHC Copper confirmed that almost close to 100% of the work done during high strain rate deformation is converted to heat. The next important characteristic of ASBs is the width of the band, which range approximately from 10^1-10^2 μm. The width of the band depends on the hardness of the material regardless of the type of the shear band. Basically, the shear band becomes narrower as the hardness of the material increases. In general, an ASB can be described as a very thin band with extremely high strain rate, strain and temperature. These bands are harder and more brittle than the rest of the material and as mentioned earlier, they are usually preferred paths for failure, either by ductile void nucleation, growth and coalescence, or by cracking.

In previous studies, two types of adiabatic shear bands have been observed in metallic materials, namely the deformed shear band and the white-etching shear band which are described in the following sub-sections.

2.1.2.1 The Deformed Shear Band

The deformed shear band can be described as a region of intense plastic deformation in a form of flow localization caused by the destabilizing effect of thermal softening [4]. The deformed band, which most often occurs at a very first stage of shear deformation, has similar appearance to the bulk material. It consists of highly distorted and elongated grains parallel to the direction of applied shear stress (Fig. 2.4) and it commonly forms in low density materials such as copper and aluminum alloy as well as denser metals including: pearlitic and ferritic steel and uranium alloys [4].

Typically, a single shear band forms as a result of a single nucleation point; but it is possible for multiple shear bands to form parallel to each other or spread homogeneously across the material if two or more nucleation points of similar size and type are within close proximity of each other or randomly spread across the material. Possible nucleation sites include precipitates, phase boundaries of two dissimilar phases, voids present within the material, scratches, machine marks or thinner sections on the specimen.

Also, it is worth to mention that the nucleation of cracks in a deformed shear band is not as easy as it is in a white-etching band due to the higher ductility of deformed shear band than white-etching band. Therefore, the material that contains deformed shear bands can withstand the impact wear better than the one containing white-etching bands [11].

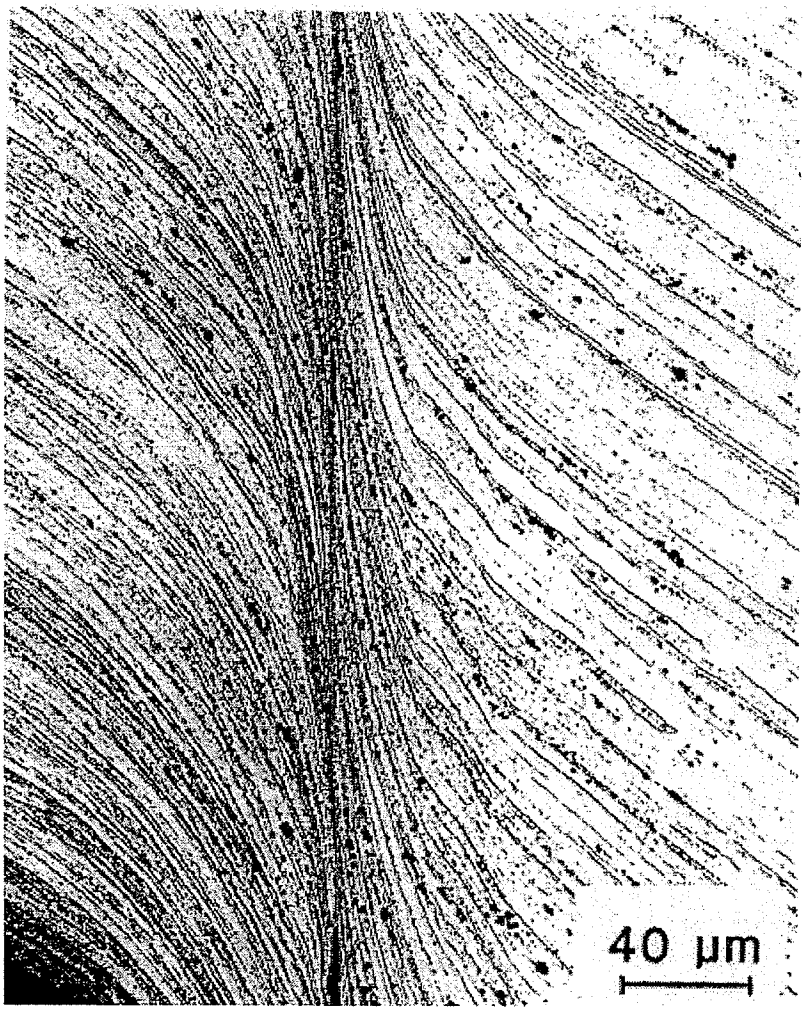

Fig. 2.4: Detail of shear band formed in aluminum alloy with a plate of hardness 80 HV, impact velocity 311 m/sec, magnification x 388. After Leech, P. W. (1985), *Metallurgical Transactions* 16A, 1900-1903 published by permission of American Soc. of Metals and Minerals, Metals and Materials Soc. [12]

2.1.2.2 The White-Etching Shear Band

The white-etching shear band, also known as transformed shear band, consists of very fine sub-grains, which has very different appearance than surrounding bulk material. It is obvious from the name that this band appears as a white band (Fig. 2.5). This white nature of ASB is found to be due to two main reasons: 1. phase transformations that produce a permanent change in microstructure, 2. the resolution limit of optical microscopy in resolving the nanometer substructure of the shear bands. The transformed band commonly forms in quench and tempered steels and it was first explained by Zener and Hollomon (1944) [4]. From measuring the hardness of the band and comparing it to the rest of the material, Zener and Hollomon have concluded that the white etching band in steel results from the transformation of austenite to martensite [4].

In many cases, both white etching and deformed bands can be observed in microstructure of the materials, depending on the deformation conditions. As shown in Fig. 2.6, the deformed band appears in region ahead of the tail end of the white etching band in the microstructure of a steel sample after impact. Li G. A. *et al.* [13] concluded that as the shear strain increases, the width of the band decreases, which results in transformation of deformed band to white-etching band.

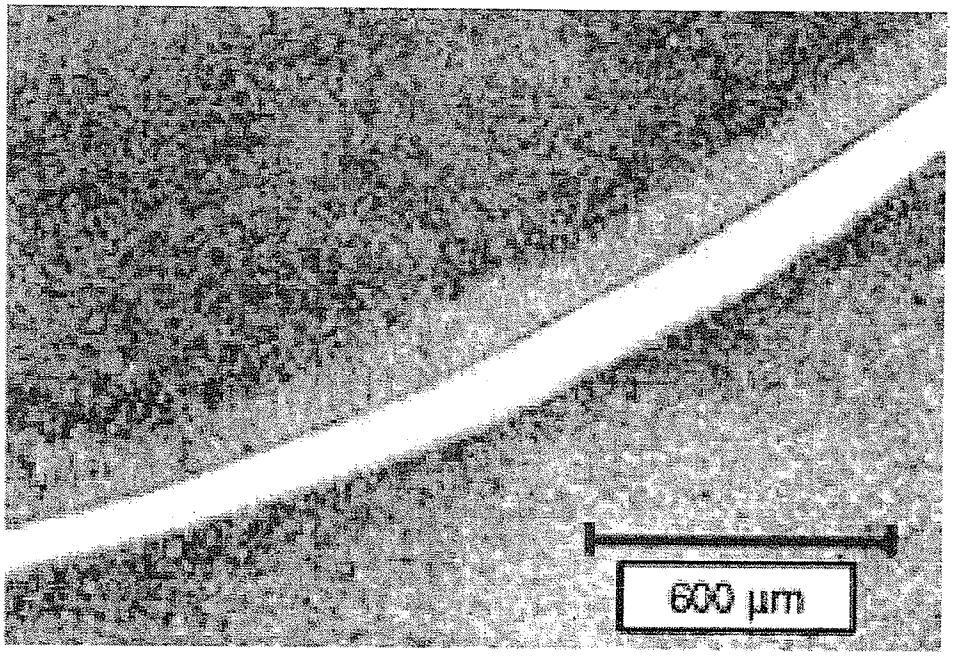

Fig. 2.5: Schematic of White-etching band (Transformed band) in AISI 4340 steel. [7]

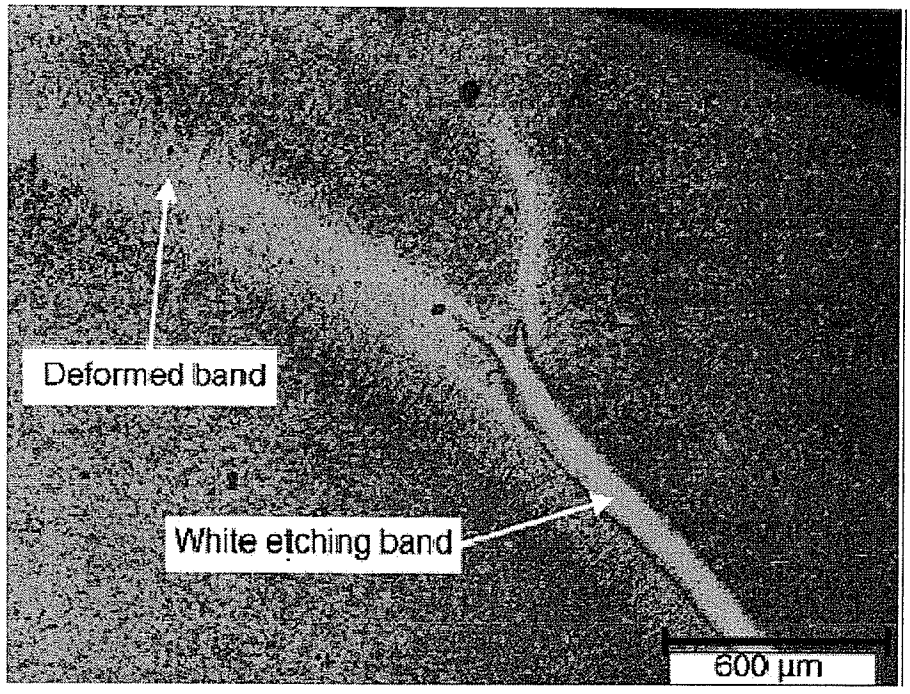

Fig. 2.6: Optical micrograph showing white etching band and deformed band in the microstructure of a steel sample after impact [7]

2.1.3 Microstructure Aspects of Initiation and Propagation of Adiabatic Shear Bands

The initiation and growth mechanisms of adiabatic shear bands are best understood by analyzing the microstructure evolution at the tip of the bands. So far, several possible shear band initiation mechanisms have been identified in single phase homogenous materials. Fig. 2.7 clearly illustrates few possible microstructural initiation sites and they are as follows: (a) grain size inhomogeneity, (b) geometrical softening, (c) Peirce-Asaro-Needleman textural localization, (d) dislocation pile-up release. Basically under dynamic loading, the larger grains, as a result of having lower yield stress than smaller grains, can act as a preferred site for initiation of shear bands. The geometric softening caused by crystallographic rotation can also play an important role in initiation of shear bands by creating localized softening in single crystals [14, 15]. The third mechanism was initially studied by Pierce *et al.* [16], then by Anand and Kalidindi [17] and finally reviewed by Nesterenko *et al.* [15]. This mechanism basically states that the localized deformation of a grain can result in extended strain localized band through cooperative plastic deformation of grains. Lastly, a dislocation pile-up can break through a grain boundary, causing a local rise in temperature and softening, which creates a site for shear band initiation.

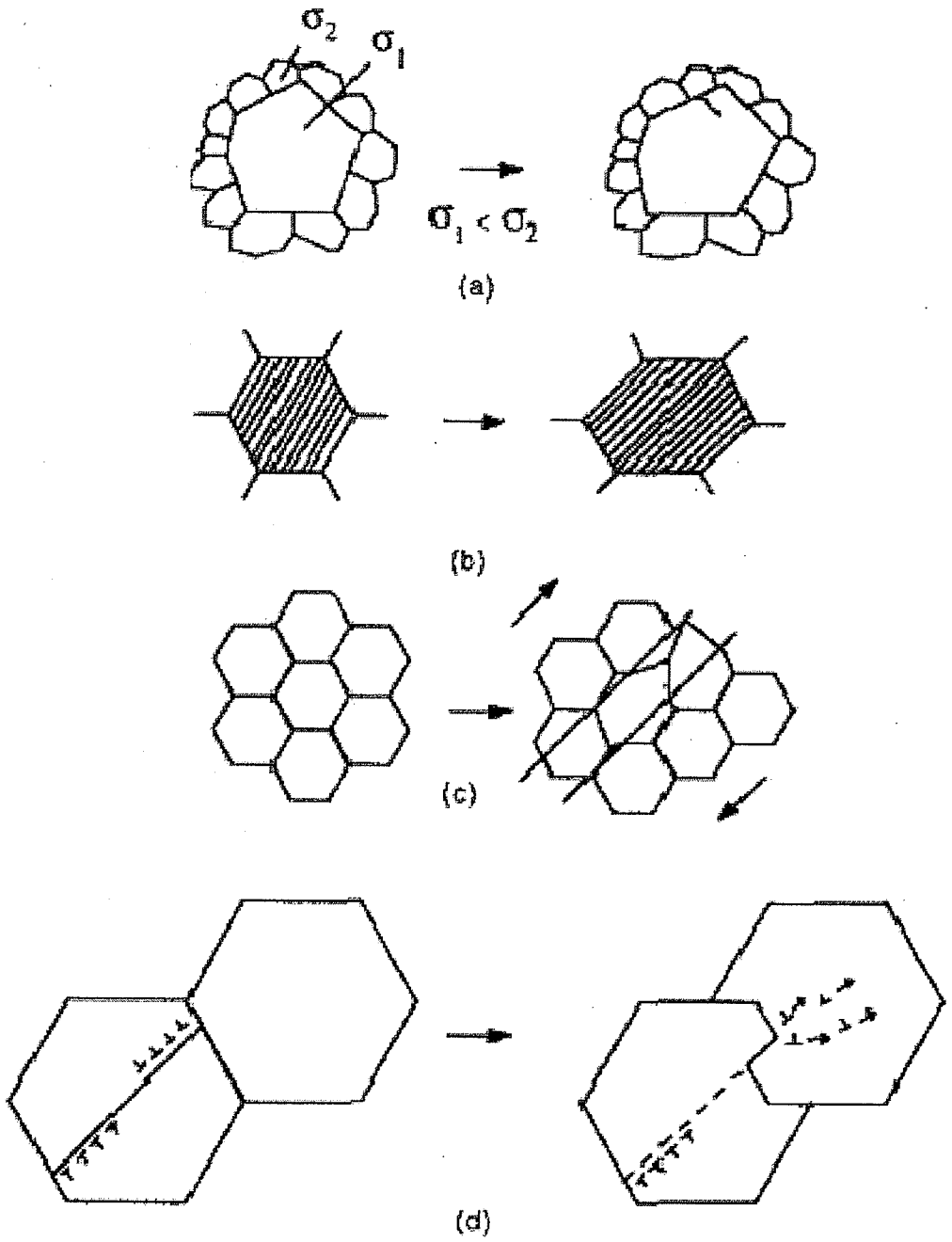

Fig. 2.7: Possible shear-band initiation mechanisms in single-phase homogeneous materials: (a) grain size inhomogeneity; (b) geometrical softening; (c) Peirce-Asaro-Neddleman textural localization; (d) dislocation pile-up release [15]

Investigation on copper single crystal by Li S. X. *et al.* [14] indicates that over the strain rate range of 2-9 x 10^3 s^{-1}, the dominant micro-deformation mechanism is dislocation motion. Fig. 2.8 represents appearances of ASBs in copper after dynamic loading (Fig. 2.8a) using scanning electron microscope (SEM). In the second figure (Fig. 2.8b), the initiation of ASB resulting from the deviation of the persistent slip bands (PSBs) can be seen after close examination of the sample surface. Persistent slip bands, among many slip bands, form during cyclic deformation and have a corresponding characteristic dislocation pattern called the ladder structure. From this observation, Li *et al.* proposed that micro-mechanism for initiation of adiabatic shear band in single crystal copper occurs in three stages as schematically presented in Fig. 2.9. These three steps are as follows:

1. Initially, the dislocations in PSBs get affected since PSBs are soft and start to move with less resistance (Fig. 2.9b) due to the application of impact loading (Fig. 2.9a).
2. As the deformation continues, the secondary slip starts to form near the interface between the PSBs and the matrix (Fig. 2.9c) due to the rotation of the loading axis towards the duplex slip side.
3. Lastly, the formation of an adiabatic shear band takes place (Fig. 2.9d) by dislocations breaking through the network in a suitable direction. This is due to the increase in both dislocation density and the required stress to overcome dislocation barriers.

Fig. 2.8c and 2.8d respectively illustrate the elongated cell structure of ASBs at the initiation stage and during propagation as these cells become elongated subgrains.

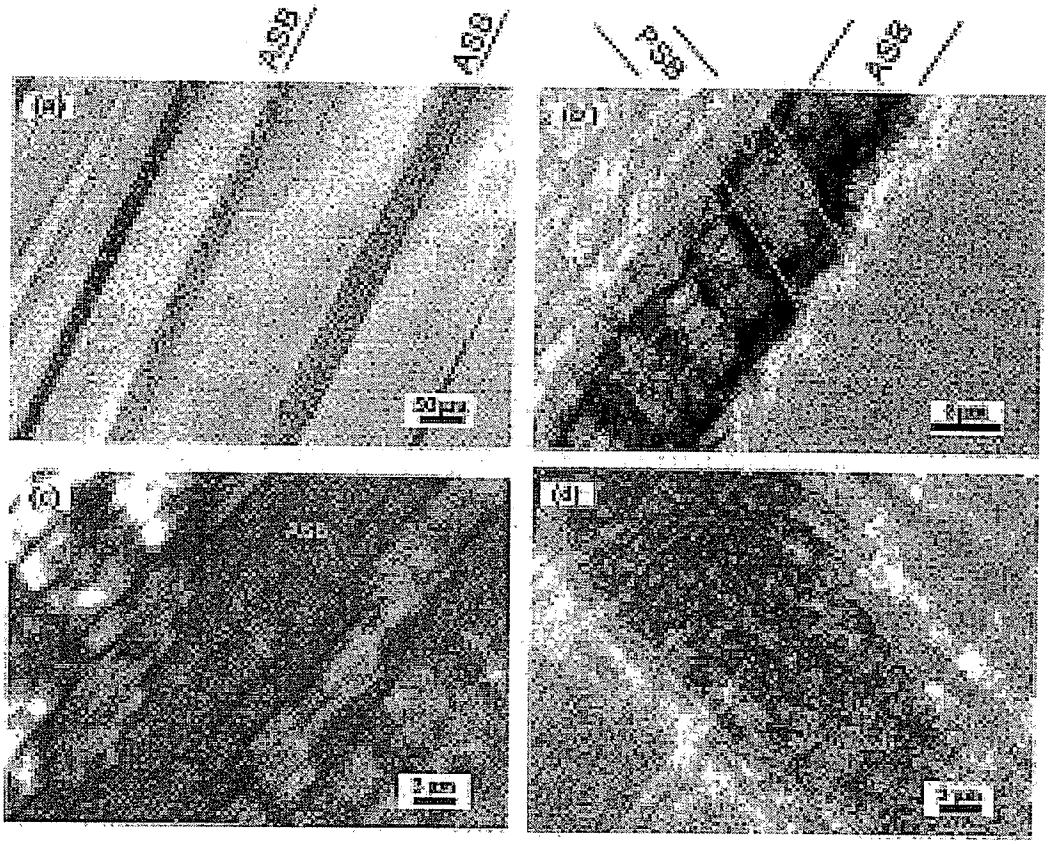

Fig. 2.8: Appearances and microstructures of different copper single crystals observed by SEM-ECC technique: (a) ASBs in SC-B; (b) shearing of an ASB results in the PSBs deviating from their original direction by about 10° in SC-B; (c) ASB microstructure in SC-C; (d) ASB microstructure in SC-D [14]

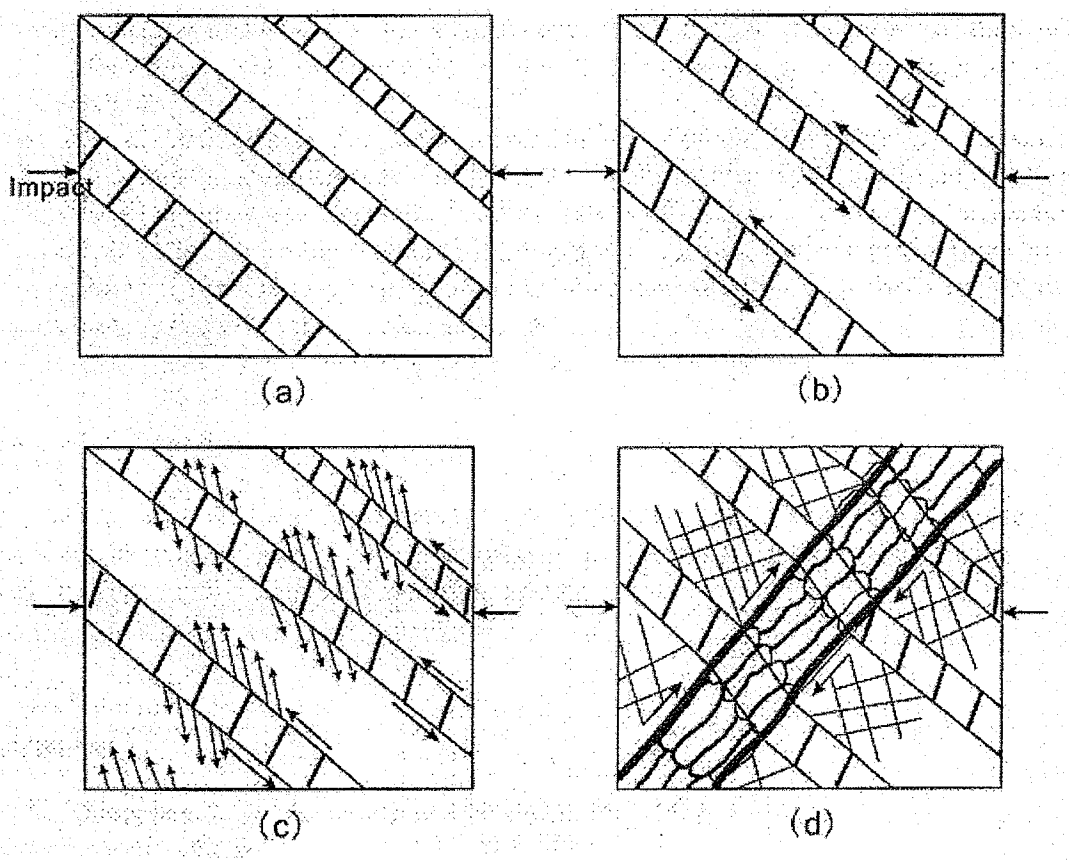

Fig. 2.9: Schematic of ASB formation in a fatigued copper single crystal [14]

The mechanisms for recrystallization under high strain and high strain rate conditions within shear bands are somewhat unclear. Several investigators including Meyers *et al.* [18] and Chichili *et al.* [19] have managed to illustrate a model for the microstructural evolution of ASBs during severe plastic deformation. This model is schematically presented in Fig. 2.10, which clearly shows the sequence of the formation of ultrafine grain size. Originally, there is a homogenous distribution of high densities of both dislocations and twins (Fig. 2.10a). As the twins near the boundary of the shear band start to disappear, the grouping of dislocations to form subgrain walls occur (Fig. 2.10b). Gradually, the misorientation between these cell walls, which act as a barrier for dislocation propagation, increases (Fig.2 10c), resulting in further division of elongated subgrains into equiaxed subgrains (Fig. 2.10d). In the last stage (Fig. 2.10e), the development and reorientation of equiaxed subgrains happen and ultrafine grains generate.

Hines and Vecchio [20] also concluded the similar mechanisms, as mentioned above for the recrystallization within ASBs in medium to high stacking fault energy materials such as copper. They observed small recrystallized grains (0.1-0.2 μm diameter) in ASBs of shock-prestrained copper.

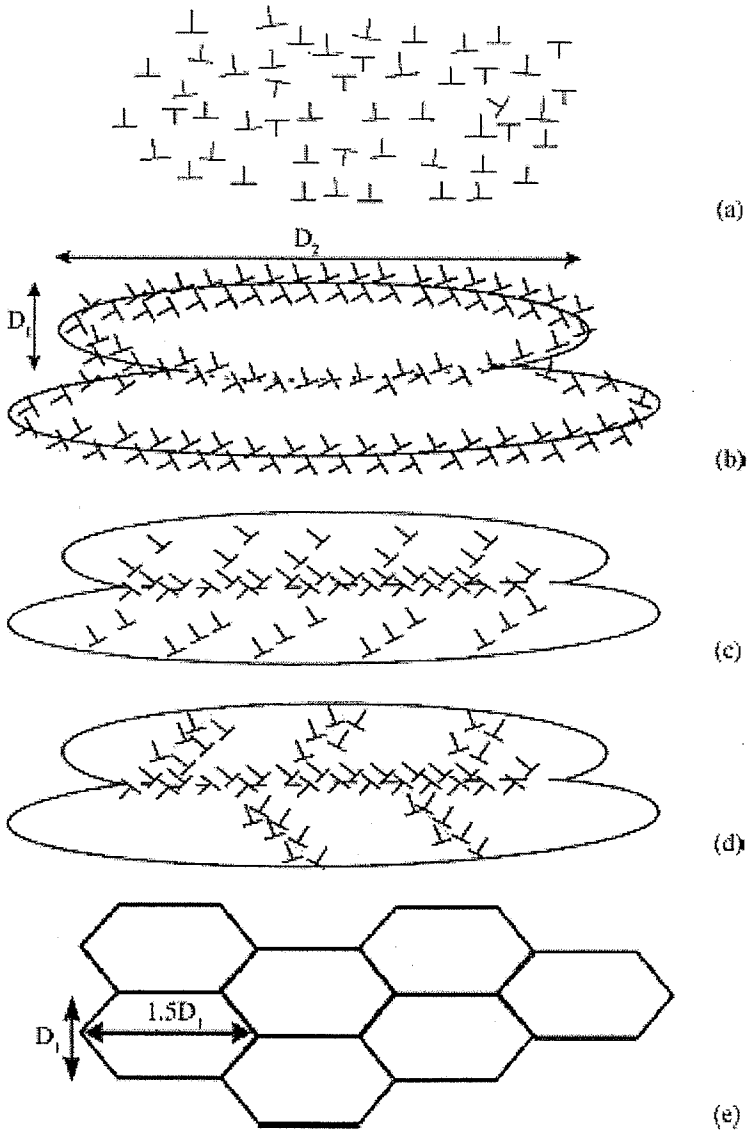

Fig. 2.10: Schematic illustration of microstructural evolution during sever plastic deformation: (a) Homogeneous distribution of dislocation; (b) elongated cell formation; (c) dislocations blocked by subgrain boundaries; (d) break up of elongated subgrains; (e) reorientation of subgrains boundaries and formation of ultrafine grain size [18]

2.1.4 Factors Influencing the Formation of Adiabatic Shear Bands

The formation of adiabatic shear bands in materials depends on numerous parameters such as: external loading conditions, material microstructure including size and orientation of grains, thermal diffusivity, rate of strain hardening and thermal softening, strain rate, strength level, specimen geometry and etc [4, 21, 22]. But, due to the extreme diversity of these factors, only the few most important ones are discussed here. In general, it can be concluded, based on the work of many researchers that adiabatic shear bands form readily in materials with low thermal diffusivity, low strain hardening coefficient, high thermal softening and high strength/hardness value.

According to Zener and Hollomon (1944) [3], the thermal softening and strain hardening are the two major material parameters affecting adiabatic shear band formation. Thermal softening mostly favors adiabatic shear and for this reason, the material with low thermal conductivity have higher improbability of forming ASBs. It can also be seen in Fig. 2.11 [23], that high conductivity materials such as aluminum and copper usually do not undergo shear localization. The black solid circles in this figure represent materials which form transformed bands, half black circles represent deformed bands and white circles represent materials which most often do not form any type of shear bands. At the same time, the more the strain hardening, the greater the degree of resistance to shear banding, which in turn, requires a high strain to overcome this resistance and create preferred sites for initiation of ASBs. [4]

● = form transformed bands
◗ = form deformed bands
○ = often do not form any type of bands

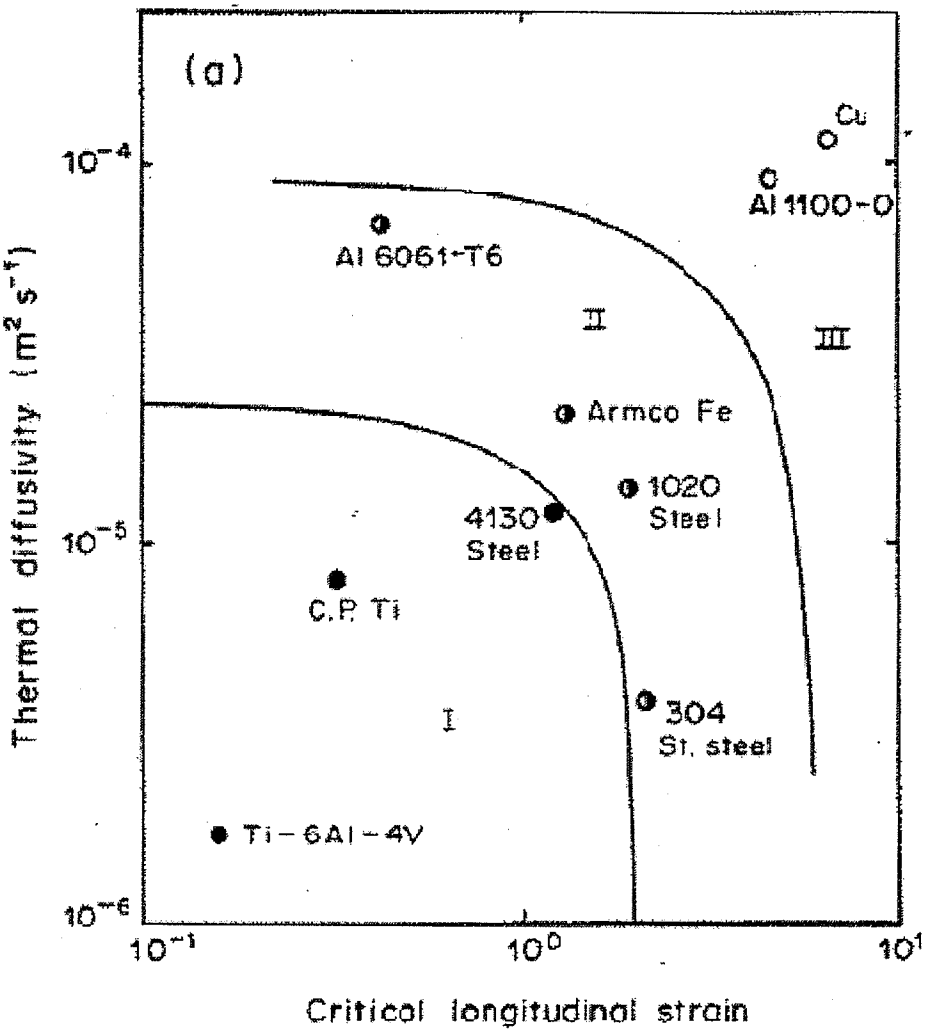

Fig. 2.11: Thermal diffusivity vs. Critical longitudinal strain, showing material parameters influence on shear band type [23]

Studies by Marchand and Duffy [6] and many others indicate the significant role that microstructure of metals plays in the initiation and propagation of ASBs. It has been reported that the presence of defects, impurities and inhomogeneities in structure can promote adiabatic shear bands formation. For example, Schonefeld and Wright [2] and Feng and Bassim [24] have observed that shear strain localization occur at the most non-uniform part of the microstructure and propagates due to the presence of material and geometrical defects.

The grain size is one of the most important parameters that affect the strength of materials. It was found by Schmidt *et al.* [25] that at low shear strain (below 0.7), the grain size has a very small effect on the stress-strain behavior of copper at high strain rate; whereas, at higher shear strain (above 0.7), coarse grained material exhibits more rapid strain softening and less ductility than fine grained material due to their higher percentage of surface irregularities. It is because of these rough surfaces that a sizable geometric differences form in the thickness of a thin member of the Torsional Split Hopkinson bar specimen and create instability sites for the formation of ASBs.

The strain rate $\dot{\varepsilon}$ sensitivity of the flow stress of many materials varies strongly above their critical value $\dot{\varepsilon}_c$ than below it (Fig. 2.12). The investigations by Gorham [26] on copper and many other investigators show similar correlation between specimen dimensions and the variation in strain rate critical value. These results are summarized in Fig. 2.13, which illustrate that lower values for $\dot{\varepsilon}_c$ are associated with the larger specimens and the higher values with the smaller specimens. Li *et al.* [14] concluded that the critical strain for the formation of ASB is orientation dependent in copper single crystal.

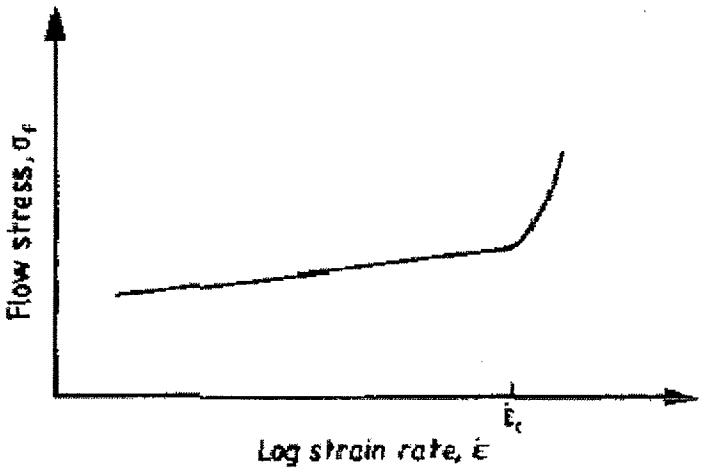

Fig. 2.12: Stress/strain-rate relationship that is typical of many metals [26]

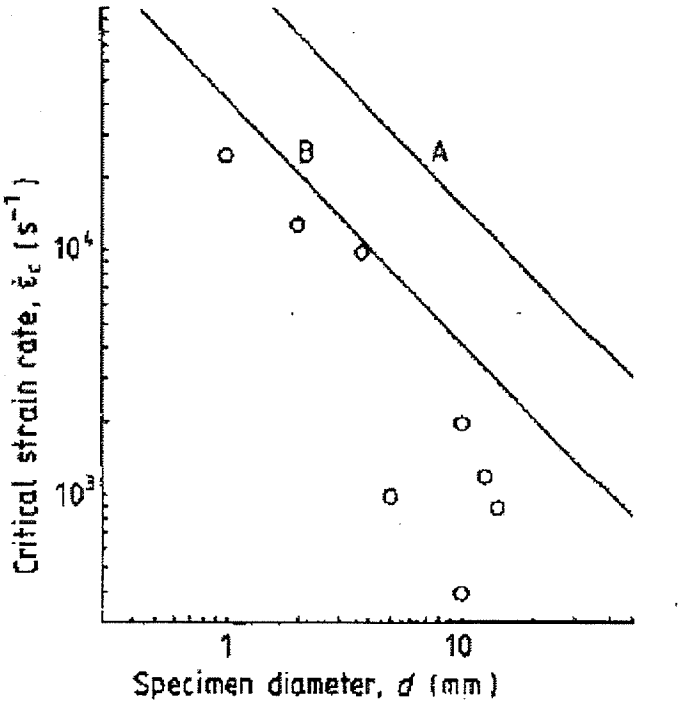

Fig. 2.13: Values of the transitions strain rate $\dot{\varepsilon}_c$ plotted against specimen diameter [26]

2.1.5 Failure at Adiabatic Shear Bands

Developing a good understanding of how the loading condition and microstructural features influence micro-failure in materials is very important, especially in designing more failure-resistant structure. However, the occurrence of fracture within a material is not a single simple process. As described earlier in this chapter, adiabatic shear bands are often preferential paths for failure, either by ductile void nucleation, growth and coalescence, or by cracking. Generally, there are two types of fractures: brittle fracture and ductile fracture. If fracture is ductile it will have occurred during the formation of the adiabatic shear band when the band was still hot; whereas brittle fractures occur after deformation in the cool band [4]. Most often, cracks are associated with brittle materials and voids with ductile materials.

Adiabatic shear bands have lower flow stress than the surrounding material at the beginning of their formation as a result of the high temperature that is generated during impact testing. Therefore, these bands are similar to ductile material and become favorable sites for void nucleation (Fig. 2.14). However, after the deformation is completed, adiabatic shear bands regions become harder than the rest of the matrix, which in turn make these bands more brittle and more susceptible to cracking (Fig. 2.15)

Study by Xue *et al.* [27] on Ti-6Al-4V alloy demonstrates the three main stages during void evolution (Fig. 2.16). Initially, voids are nucleated within a shear band and gradually grow to the width of the band. Following this stage is the elongation and rotation of voids along the direction of the shear band. Finally, the voids coalesce and create cracks.

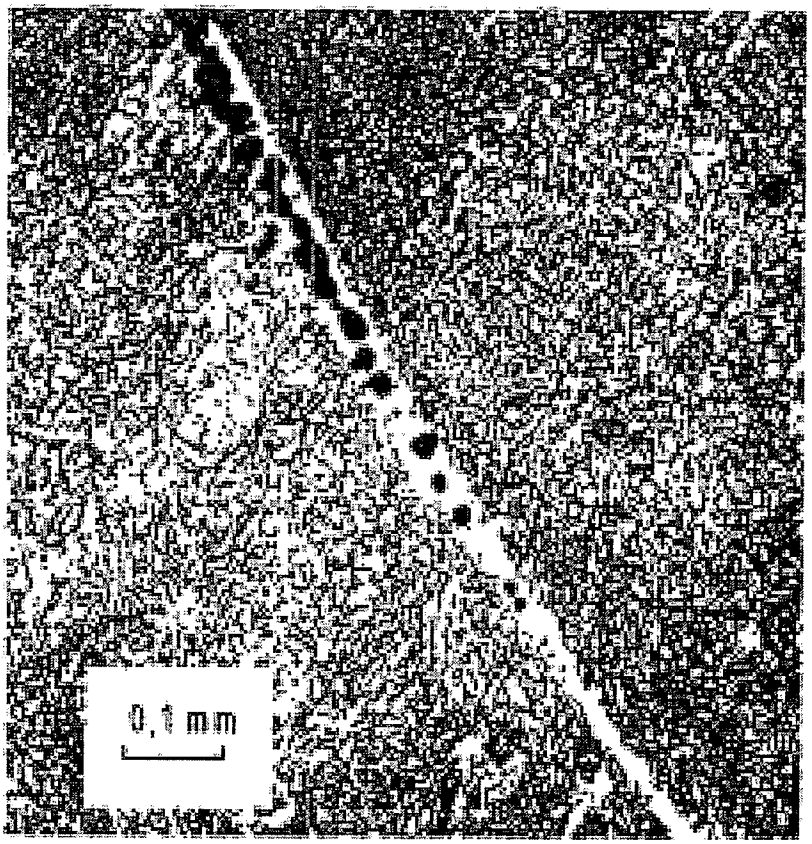

Fig. 2.14: Ductile fracture appears as coalescence of microvoids in a U-2Mo alloy [4]

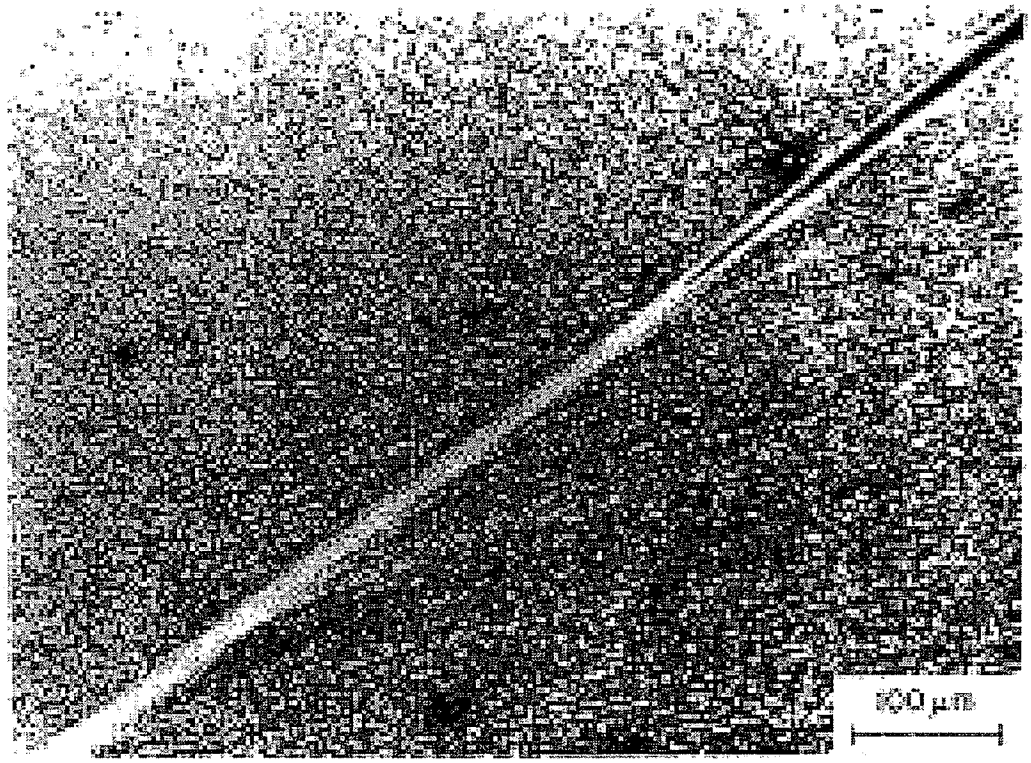

Fig. 2.15: Brittle fracture appears as a sharp crack within a transformation band in a martensitic steel deformed in dynamic compression test [4]

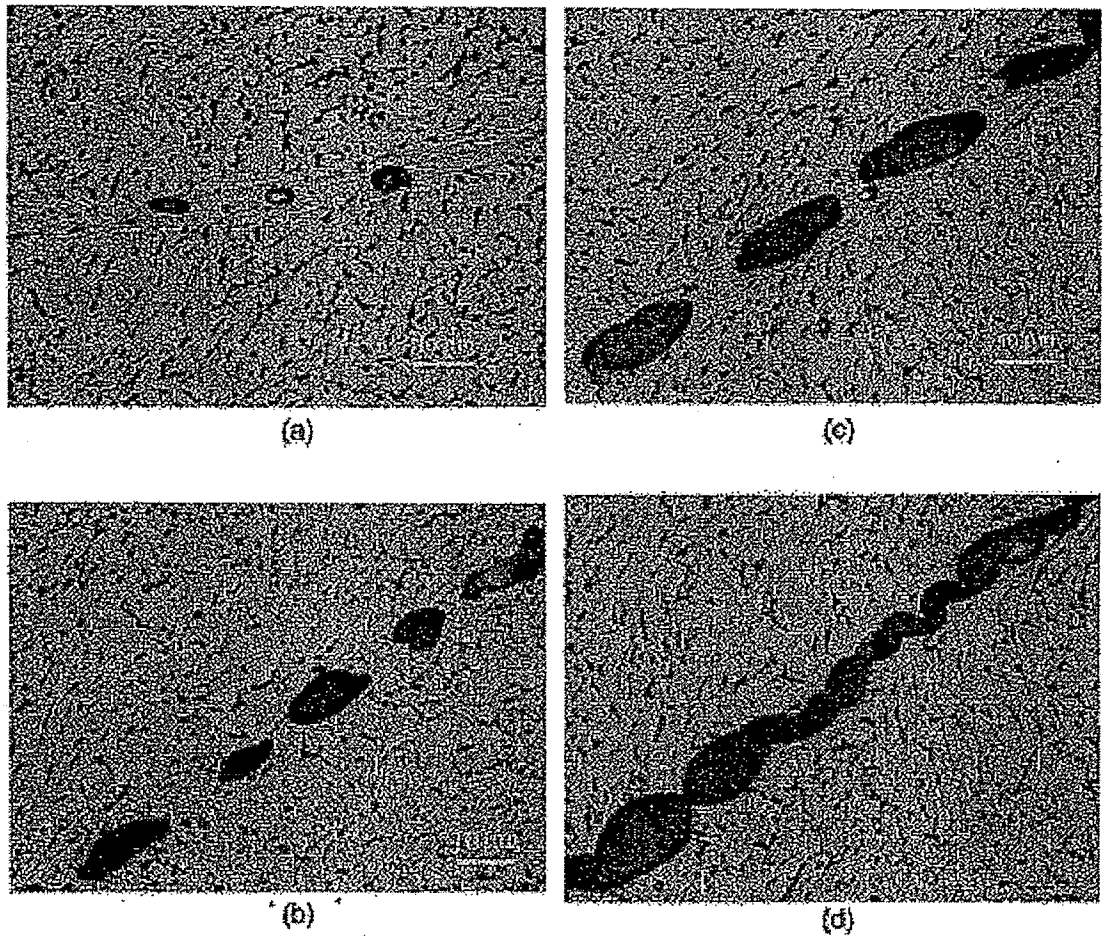

Fig. 2.16: Void nucleation and growth inside a shear band in Ti-6Al-4V alloy: (a) nucleation of voids within a shear band; (b) growth of voids; (c) elongation and rotation of voids; (d) coalescence of voids to from crack [27]

Examining the failure mechanism from a submicroscopic level shows the important role that the density and movement of dislocations play during deformation. Microvoids and microcracks are nucleated due to the dislocation pile-up that forms against the obstacle, like grain boundaries, as a result of slip that occurs by the movement of dislocation during deformation [28]. The connection between the brittle and ductile failures with the no-release or release of dislocations, respectively, are presented in the work of some researchers such as Stroh (1957) [29] and Curran *et al.* (1987) [30]. Their works essentially imply that when the dislocations tangle up at one point with not much movement, tensile stresses are created which contribute to brittle failure. In ductile material, the plastic deformation is produced by the release of dislocations that in turn causes delay in occurrence of fracture until the plastic strain reaches a critical value. Therefore, in order to reduce failure in material, finding this critical value of plastic strain is the main key factor.

For copper, because of its high ductility, the fracture usually takes place either by void nucleation or slip or both and most often stress in tensile form or very high stress rate is required. Investigation by Meyers *et al.* [31] suggests that the nucleation and growth of voids in copper occurs as a result of a large dislocation density that surrounds the void edges and introduces plastic deformation. They have also showed that the nucleation of voids in copper is grain size dependent. As shown in Fig. 2.17, the homogeneous nucleation occurs throughout the copper if the grain size is small and for larger grains, the nucleation is primarily along the grain boundaries.

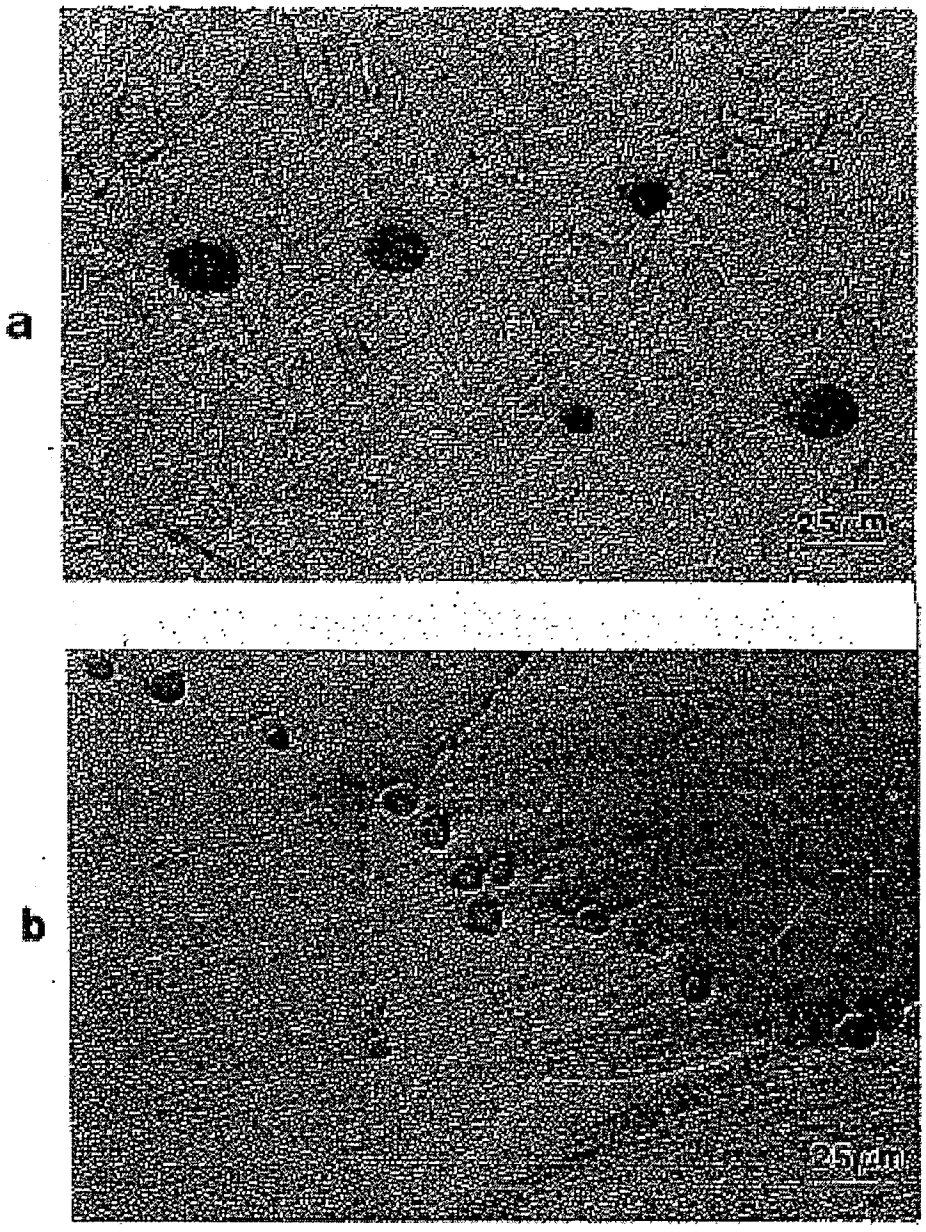

Fig. 2.17: Effect of grain size on void distribution in copper; (a) specimen with G.S. = 20 μm, (b) specimen with G.S. = 250 μm [31]

2.2 The Torsional Split Hopkinson Pressure Bar Testing Method

High strain rate testing on basic materials is very important in most engineering applications and metalworking operations. Therefore, the testing techniques should create a high enough strain rate in the specimens. These techniques can also be used to study the adiabatic shear bands formation in materials.

Several methods have been developed for high strain rate testing including the Hopkinson Pressure bar, which first developed by John Hopkinson and his son, Bertram Hopkinson, in 1914 [32, 33]. In 1949, based on original experiments and Davies work [33, 34], Kolsky introduced the Split Hopkinson Pressure bar (the Kolsky bar), in which the specimen is sandwiched between an input and output pressure bar and is deformed in such a way that there is no stress gradient along the sample [33, 35].

The Split Hopkinson bar is now available in tension [36, 37], compression [36] and torsion [38]. Baker and Yew were the first ones to introduce Torsional Split Hopkinson bar in 1966 [4, 39]. Testing materials in the 10^2 to 10^4 s^{-1}strain rate range can be achieved using this equipment. Also, when it comes to testing materials under large dynamic plastic flow, torsional loading has more advantages over any other forms. This is discussed in the following sub-section.

2.2.1 Advantages and Disadvantages

One of the most important advantages of the torsional test over any other available forms of testing techniques is that a homogeneous shear deformation without any major macroscopic changes in tested specimens, such as radial expansion or contraction that are generated during compression or tensile tests can be produced using

torsional loading. Also, there are no inertial or frictional effects in torsion as a result of the absence of a Poisson ratio effect.

Another important advantage of the torsional over the direct impact Split Hopkinson bar arises from the fact that there is no geometrical dispersion in the torsional pulse along an elastic bar as it reaches the specimen. This feature of the torsion test is due to the fact that the velocities of the frequency components present in the torsional pulse are the same, unlike the ones in the compression pulse. As a consequence of the absence of geometrical dispersion in torsion, any restrictions present in the direct impact test, regarding the strain gage stations locations on the incident or transmitted bars to capture the correct pulses are dismissed. [4, 33, 39]

On the other hand, certain disadvantages are associated with the torsional Split Hopkinson bar that must be considered. In general, there is a limit to the amount of torsional loading that can be applied due to the limitation to the amount of torque that can be stored in incident bar. Therefore, much lower strain rate can be achieved during torsional loading compared to impact loading. Machining tubular test specimens is more complicated and expensive. Gripping these tubular specimens tightly between the two elastic bars without damaging them is very difficult as well. Also, any other shaped specimens other than circular are unsuited for torsional test. Overall, the torsional Kolsky bar is considered to be more costly to build and implement than the direct impact Kolsky bar. [4, 33, 39]

CHAPTER 3 – EXPERIMENTAL PRECEDURE

3.1 Material Investigated

The material used in this study is polycrystalline copper with purity of 99.94%. Copper is a face centered cubic material with a moderate to high stacking fault energy of 78 mJ m^{-2} [40] and the melting point of 1356K [41]. The average grain size of copper used in this study is determined to be 700 μm using the intercept method. Besides the lack of knowledge in mechanism of plastic deformation, another reason that copper is selected in this study is due to its simplicity as well as basic microstructure that allow for better understanding the processes such as dynamic deformation at high strain rate and formation of ASBs.

3.2 Torsional Split Hopkinson Bar Apparatus

Fig. 3.1 shows a schematic layout of the Torsional Split Hopkinson bar apparatus. This machine consists of two bars, called the input (or incident) bar (Fig. 3.2a) and output (or transmitted) bar (Fig. 3.2b). These bars are each 1.829 mm long and have a diameter of 25.4 mm and they are made of aluminum 6061-T6 alloy [42]. The bars are held in place by a series of Teflon bushing, which are consecutively attached to a 4 meter long I-beam. There are two strain gages which are attached to the incident and transmitted bars at equidistance from the specimen in such a way that the overlapping of the incident and transmitted waves is avoided.

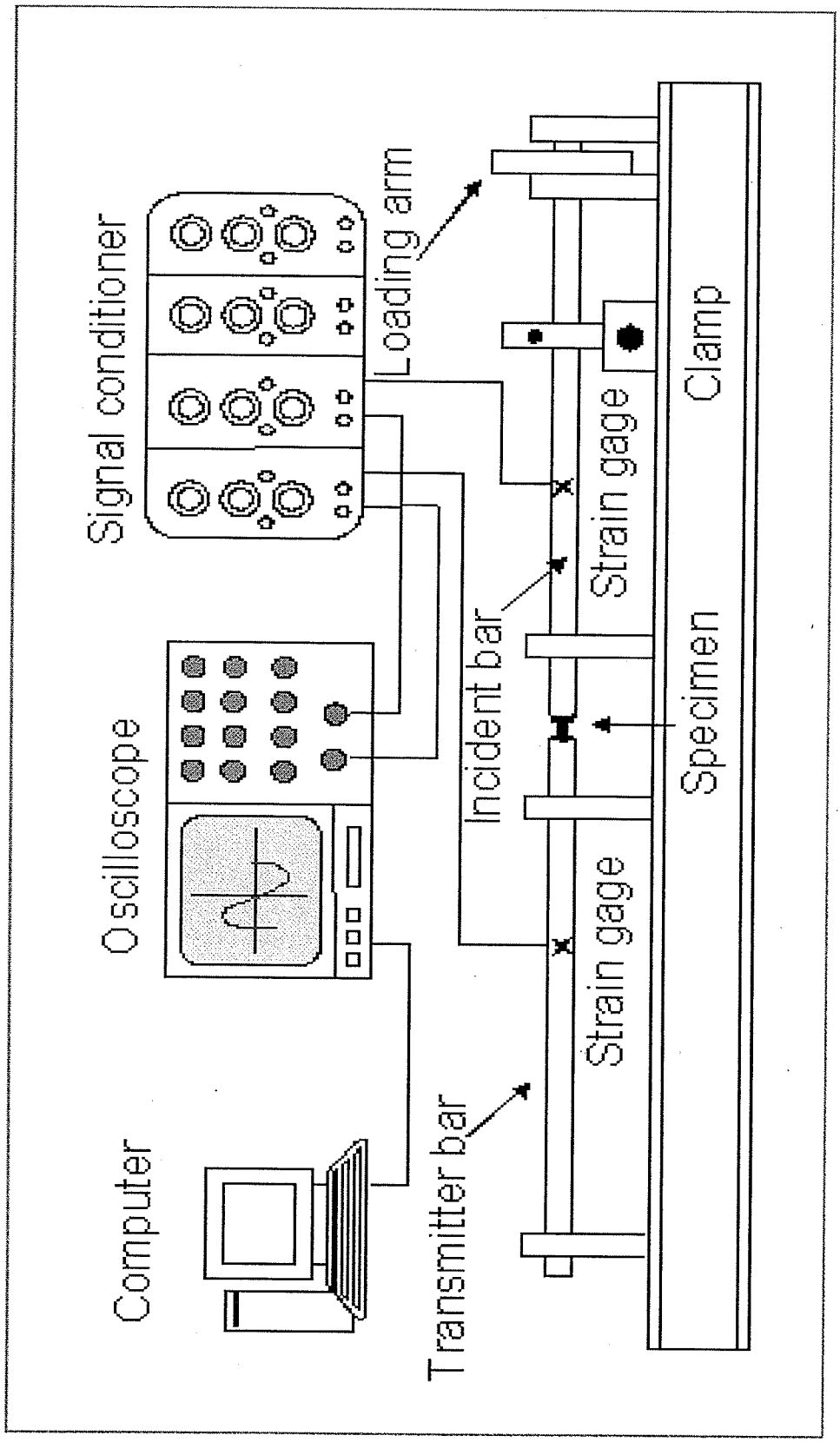

Fig. 3.1: Torsional Split Hopkinson Bar System [43]

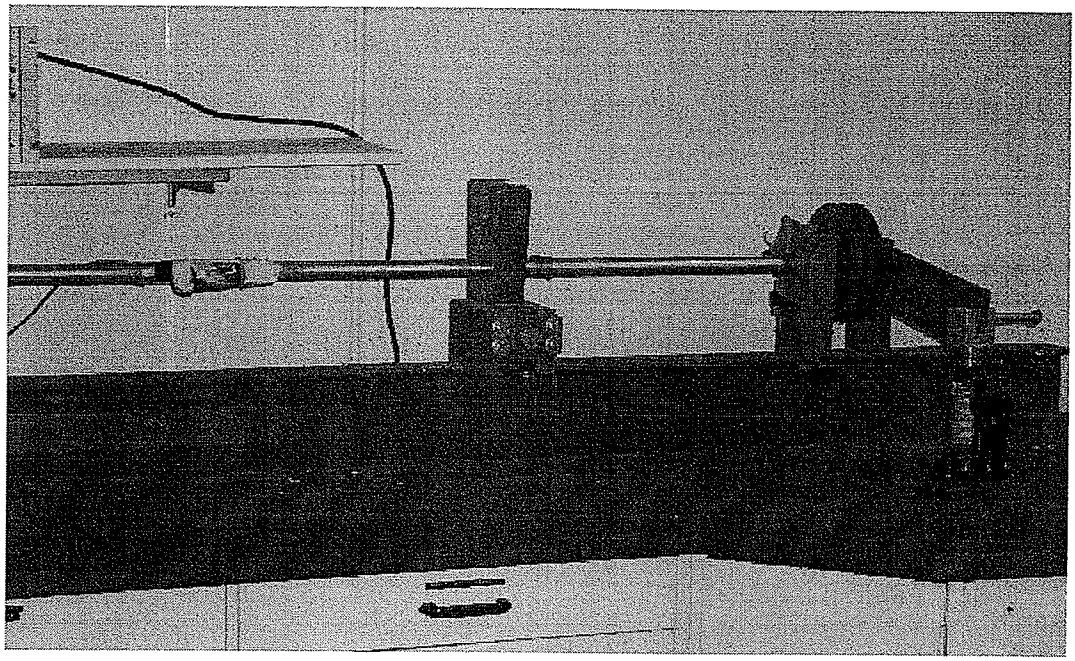

(a)

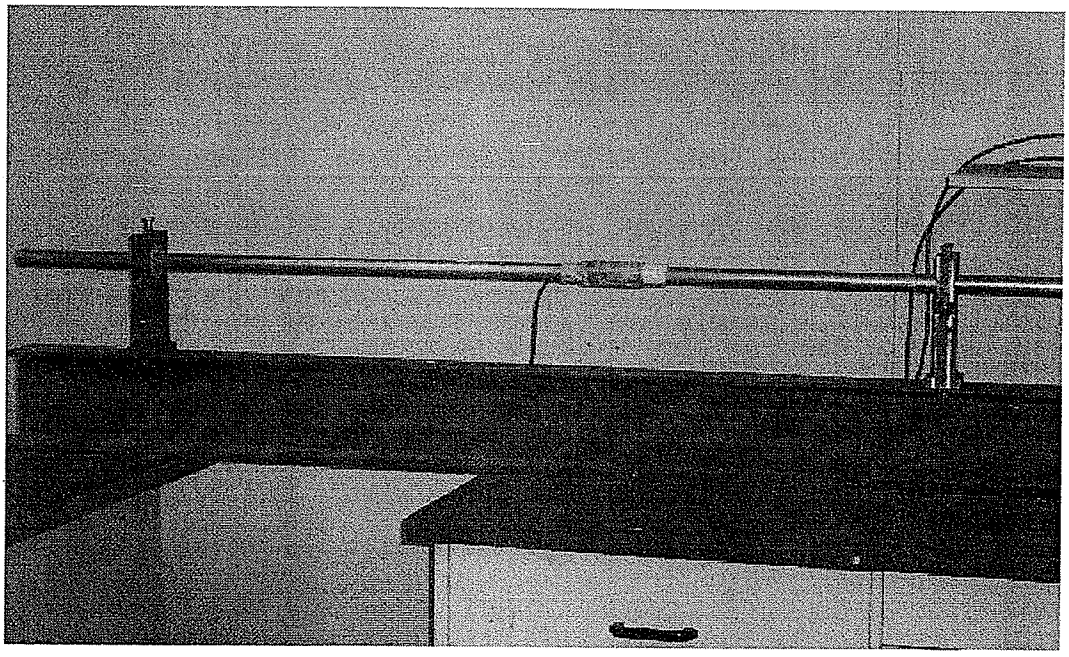

(b)

Fig. 3.2: (a) Incident bar and (b) Transmitted bar sections of Torsional Split Hopkinson bar.

In general, before dynamic testing, the torque is stored between the clamp and the loading arm. This is accomplished by first tightening the clamp to prevent rotation of the incident bar and then by applying the torsion load using a hydraulic jack connected to the rotating wheel at the end of the incident bar (Fig. 3.3). The design of the clamp has a direct influence on the quality of the loading wave. Therefore, it must be designed to be able to hold the desired torque without slipping and release this torque rapidly. [33, 43] One type of clamp design, as shown in Fig. 3.4 and 3.5, consists of two arms with hinged bottoms that press against the sides of the incident bar under the action of a notched bolt made of 6061-T6 aluminum alloy (Fig. 3.6).

The dynamic torsion test takes place when the torque is released as a result of further tightening of the clamp until the notched load release pin breaks. At this point, the generated elastic wave is partially transmitted along the incident bar towards the specimen and the rest is reflected back towards the clamp mechanism. Also, at the interface of the specimen and the incident bar, part of the wave travels through the specimen on to the transmitted bar, while another part of the wave is reflected back along the incident bar. All of these three waves (incident, transmitted and reflected) are detected and captured by the strain gages attached to the incident and transmitted bars and are recorded by a Digital Storage Oscilloscope [42] for further analysis of stress and strain curves.

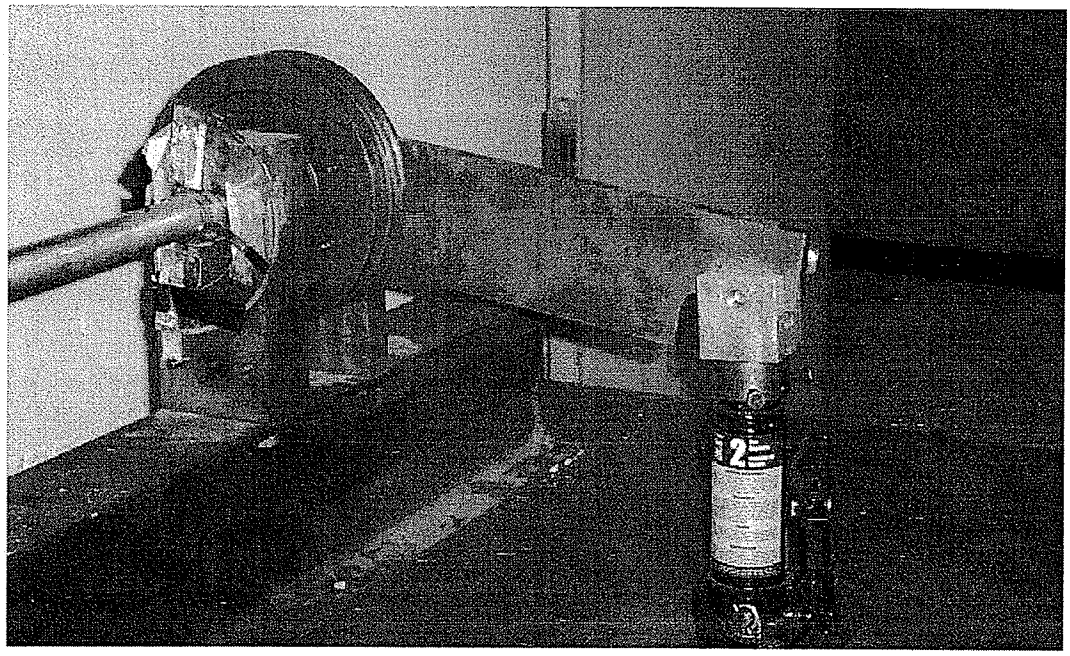

Fig. 3.3: Hydraulic jack connected to the rotating wheel

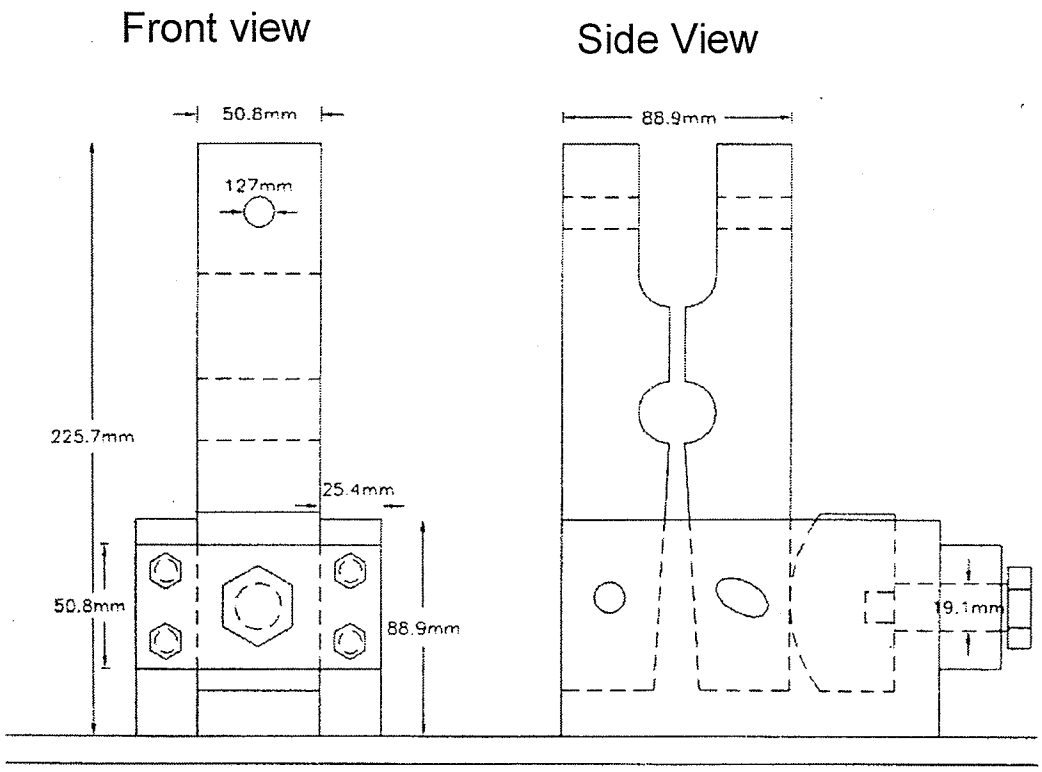

Fig. 3.4: Sketch of the clamping mechanism [23]

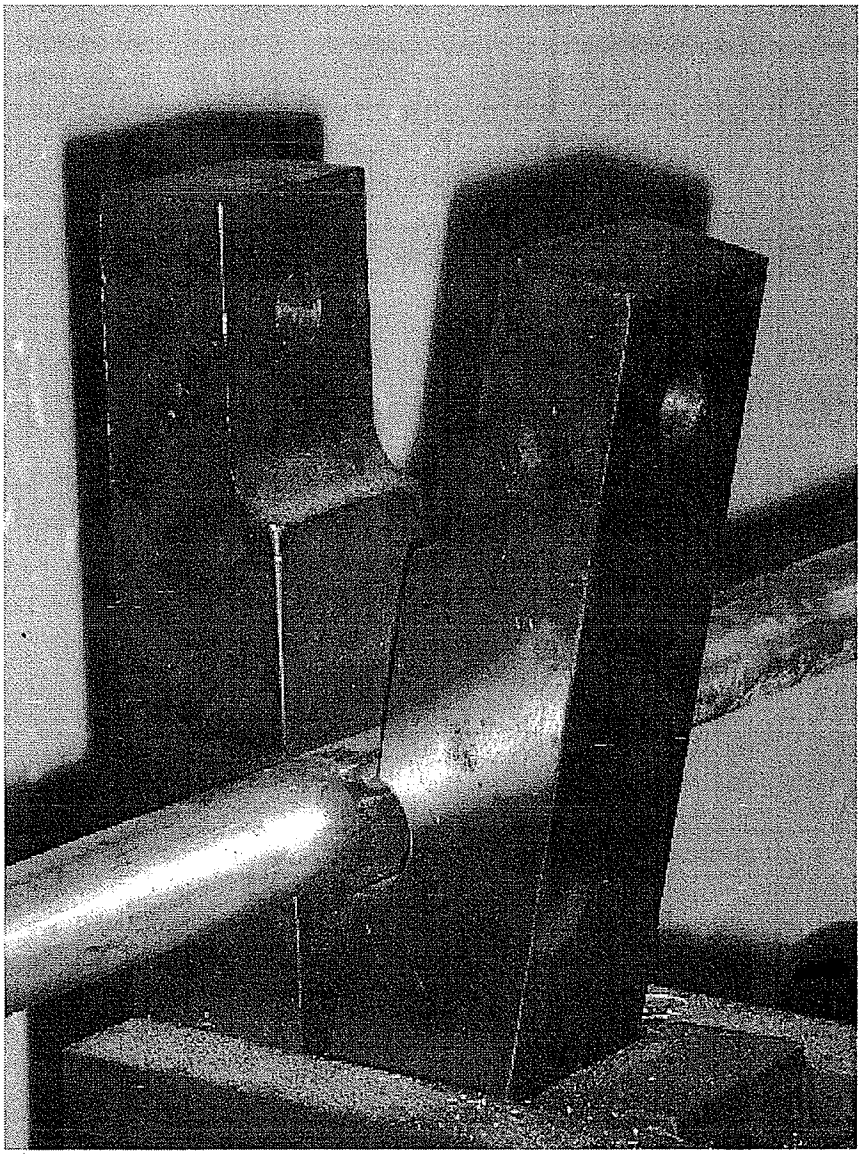

Fig. 3.5: Photograph of the clamping system

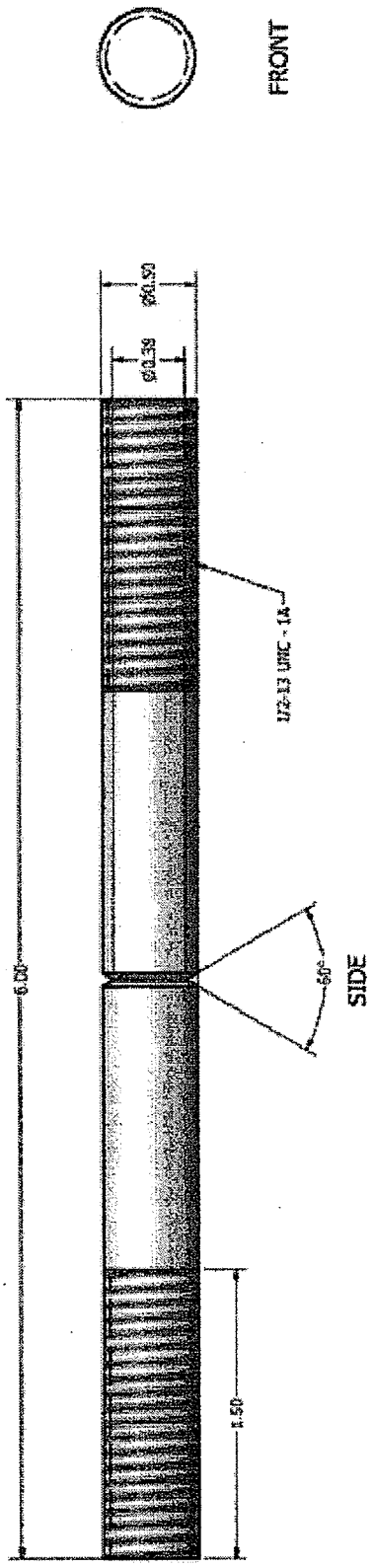

Fig. 3.6: Sketch of Load Release Pin [43]

3.2.1 Specimen Geometry and Mount

One of the important aspects of the entire experiment setup is related to the way that the sample is held between the two Hopkinson bars. The specimens used in torsional test are usually thin-walled tubes with hexagonally shaped flanges as shown in Fig. 3.7. The dimensions for each section of the specimen is established based on previous works that has been done in this laboratory by previous authors in a way that the sample satisfy dynamic equilibrium state in order to be valid in the use of the Split Hopkinson test. The end side of the incident and the transmitted bars are machined to have hexagonal sockets (Fig. 3.8) to provide means of gripping the sample with no slip between the bars and the specimens. Using this type of lock-in system eliminates the need for the use of screws or any adhesive compounds such as epoxy to hold the specimen in place [4, 43].

Twenty specimens were machined from a commercially annealed pure copper rod and subjected to torsional loading at different starting torques. The angles at which the bar was initially twisted, in order to produce different starting torques to test these copper samples, ranged between 6° to 9°. All tests were performed at room temperature and pressure. The geometry of specimens before and after torsional loading is as shown in Fig. 3.9 and Fig. 3.10, respectively. The final specimens dimensions used in this experiment are given in Table [1].

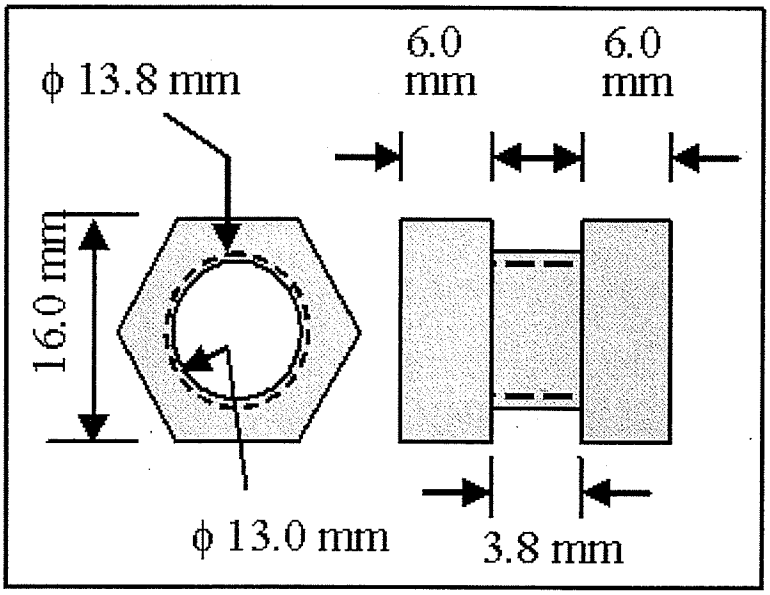

Fig. 3.7: Specimen geometry for Torsional test [43]

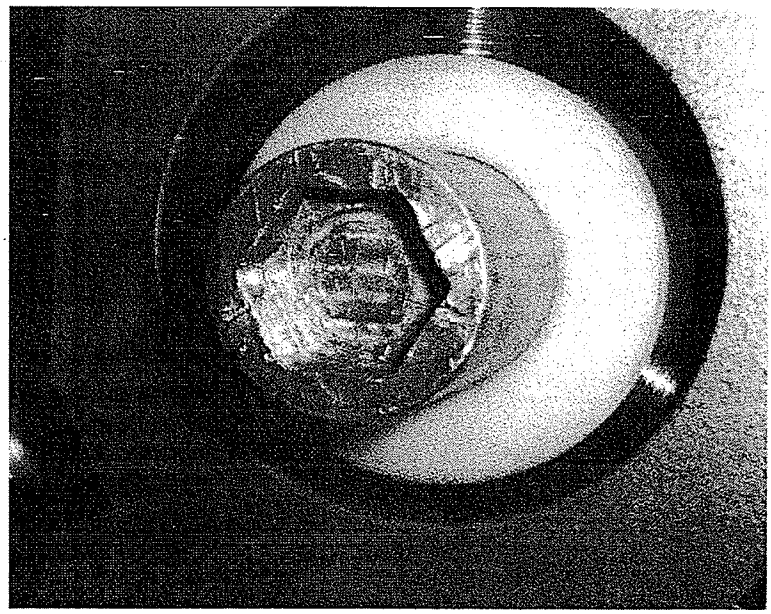

Fig. 3.8: Hexagonal socket at the end of the incident bar of Torsional Hopkinson bar [42]

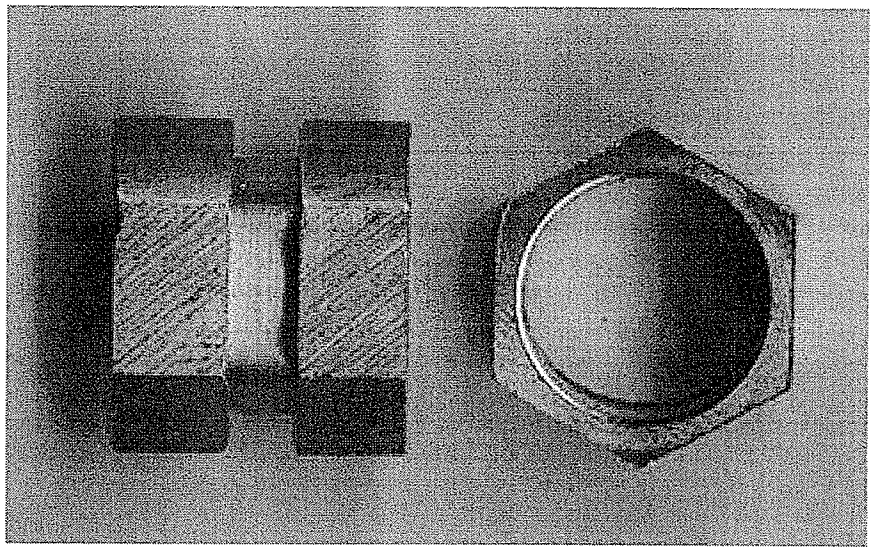

Fig. 3.9: Tubular specimen with hexagonal flanges before torsional loading

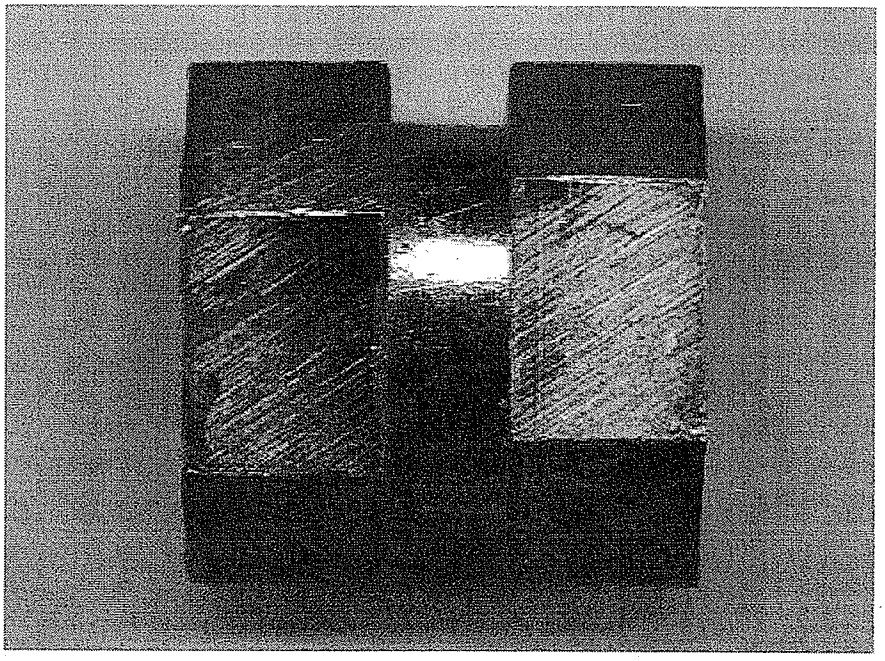

Fig. 3.10: Tubular specimen after torsional loading

Table 1: Specimen Dimensions

Twist Angle & (Torque)	*Sample #*	*Inner Diameter (mm)*	*Outer Diameter (mm)*	*Average Diameter (mm)*	*Wall Thickness (mm)*	*Gauge Length (mm)*
6° (265 Nm)	1	12.90	13.79	13.35	0.45	3.69
	2	12.84	13.88	13.36	0.52	3.70
	3	12.72	13.82	13.27	0.55	3.66
	4	12.91	13.84	13.38	0.47	3.69
7° (310 Nm)	5	12.70	13.80	13.25	0.55	3.65
	6	12.79	13.76	13.28	0.49	3.70
	7	12.85	13.84	13.35	0.50	3.72
	8	12.92	13.85	13.39	0.47	3,70
	9	12.72	13.80	13.28	0.56	3.68
	10	12.80	13.90	13.35	0.55	3.69
8° (354 Nm)	11	12.80	13.80	13.30	0.50	3.71
	12	12.70	13.82	13.26	0.56	3.68
	13	12.83	13.82	13.33	0.50	3.69
	14	12.79	13.83	13.31	0.52	3.65
	15	12.94	13.87	13.41	0.47	3.68
	16	12.90	13.80	13.35	0.45	3.68
9° (398 Nm)	17	12.96	13.83	13.40	0.44	3.69
	18	12.80	13.78	13.29	0.49	3.69
	19	12.84	13.80	13.32	0.48	3.69
	20	12.72	13.82	13.27	0.55	3.69

3.3 Calculating Stress, Strain and Strain Rate

The stress, strain and strain rate can be calculated using the incident, transmitted and reflected pulses that are obtained from the output of the strain gauges recorded in voltage vs. time format on the oscilloscope. Originally the analysis was developed in tension by Kolsky, and then transposed to shear [44]. The reflected pulse provides a measure of the shear strain rate through the specimen ($\dot{\gamma}_s(t)$) and the shear strain ($\gamma_s(t)$) in the specimen can be found simply by taking the integration of the shear strain rate while the transmitted pulse provides a measure of the average shear stress ($\tau_s(t)$) in the specimen.

The shear strain in the specimen is developed by measuring the difference in rotation between the two ends of the specimen and dividing it by its length.

$$\gamma_s = \frac{D_s\phi_2 - D_s\phi_1}{2L_s} \tag{1}$$

ϕ_1 and ϕ_2 are the twist angles in the incident and transmitter bars respectively. D_s is the mean diameter of the thin walled specimen and L_s is the gage length of the specimen. The shear strain measurement at the surface of the transmitter bar is used to determine the value of ϕ_2.

$$\gamma_T = \frac{D}{2}\frac{\partial\phi_2}{\partial x} = \frac{D}{2c}\frac{\partial\phi_2}{\partial t} \tag{2}$$

where, D is the diameter of the aluminum bars and c is the torsional velocity in the bars, which is:

$$c = \sqrt{G/\rho} \tag{3}$$

where, G is modulus of rigidity of the bars and ρ is density.

In this experiment, D is 25.4 mm and c is 3040 m/s.

From equation (2),

$$\phi_2 = \frac{2c}{D}\int_0^t \gamma_T(t)dt \tag{4}$$

Meanwhile, ϕ_1 is computed from the difference in strains due to the incidence and reflected pulses:

$$\phi_1 = \frac{2c}{D}\int_0^t [\gamma_I(t) - \gamma_R(t)]dt \tag{5}$$

The minus size is necessary because the reflected pulse travels in the opposite direction of the incidence pulse. The strain rate is determined by differentiating equation (1) and substituting equations (4) and (5):

$$\dot{\gamma}_s(t) = \frac{cD_s}{L_s D}[\gamma_T(t) - \{\gamma_I(t) - \gamma_R(t)\}] \tag{6}$$

The strain in the specimen can be determined by simply integrating equation (6):

$$\gamma_s(t) = \int_0^t \frac{cD}{L_s D}[\gamma_T(t) - \{\gamma_I(t) - \gamma_R(t)\}]dt \tag{7}$$

Simplifying equation (7) to a more workable form:

$$\gamma_s(t) = \frac{2cD_s}{L_s D}\sum[\gamma_T(t) - \{\gamma_I(t) - \gamma_R(t)\}]\Delta t \tag{8}$$

The stress is determined by the analysis of Kolsky as follows:

$$\tau_s = \frac{2T_s}{(\pi D_s^2)t_s} \tag{9}$$

where t_s and T_s are wall thickness and average torque respectively. The average torque in the specimen is related to the average torque at the interface with the incident bar (T_1) and at the interface with the transmitter bar (T_2) as follows:

$$T_s = \frac{1}{2}(T_1 + T_2) \tag{10}$$

Each one of the above torques can be written in term of strain at the surface of the bar such as:

$$T_1 = \frac{G\pi D^3(\gamma_I - \gamma_R)}{16} \tag{11}$$

The negative sign for γ_R is required due to the fact that reflected pulse travels in the negative x direction.

$$T_2 = \frac{G\pi D^3 \gamma_T}{16} \tag{12}$$

Therefore, by substituting equations (10), (11) and (12) in equation (9), the stress in the thin walled specimen is:

$$\tau_s(t) = \frac{GD^3}{16D_s^2 t_s}\left[\gamma_I(t) - \gamma_R(t) + \gamma_T(t)\right] \tag{13}$$

In the test results, equations (6), (8) and (13) are used to develop stress-strain curves, as well as to determine the strain rate.

3.4 Metallurgical Preparation and Investigation of the Material

The proper preparation of samples for further inspection is extremely important as this step is required to reveal the true microstructure in order to achieve meaningful results. This section is divided into two sub-sections: the first one briefly describes the different steps required for preparing the sample and the second one introduces the microstructure analysis methods used for examination of the samples in this experiment.

3.4.1 Sample Preparation

Sample preparation for metallographic investigation of material involves five main steps: sectioning, mounting, grinding, polishing and etching. The samples were cut in longitudinal sections using vibrating EDM machine, which is the wiring method of cutting the sample in order to create smooth cut surface. Then, the mounting press is used to make the cylindrical plastic mount around the sample using bakelite black phenolic powder. Fig. 3.11 shows both the cut section of the sample before and after mounting. The process of mounting is followed by grinding and polishing of the samples in order to obtain the mirror like surface. After grinding the sample with 1200-mesh abrasive, the sample is polished by using the 0.5 micro-meter diamond solution in addition to 6 and 1 micro-meter diamond solutions. Fig. 3.12 shows the improvement in removing scratches between 1200-mesh abrasive, 6 micro-meter and 1 micro-meter solution. At last, copper samples were etched using Ferric Chloride solution, which is a mixture of 20 gram Ferric Chloride ($FeCl_3.6H_2O$), 8 ml hydrochloric acid, 100 ml Methanol by immersion technique. In the following figure, Fig. 3.13, it can be seen that after etching the sample, a wide range of grain boundaries as well as twinning are clearly exposed.

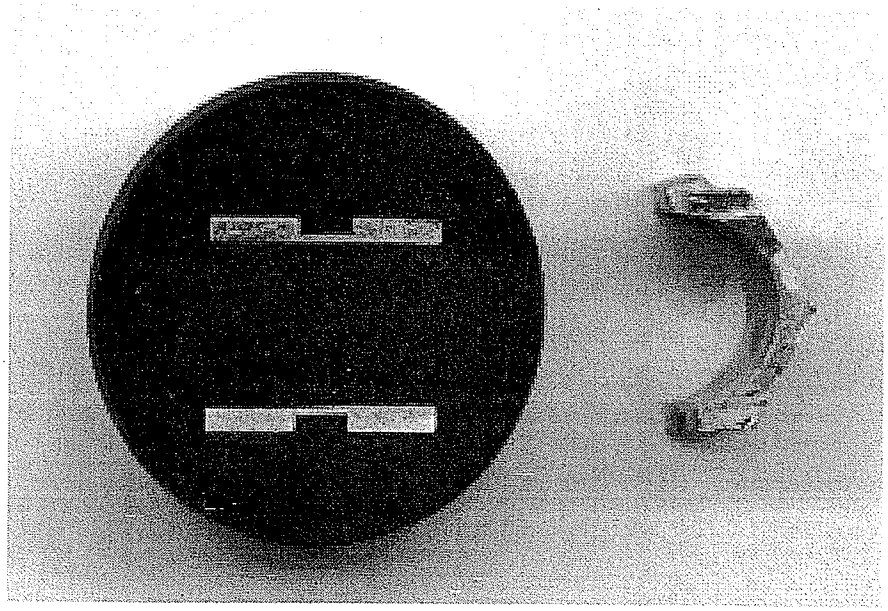

Fig. 3.11: Cut section and plastic mounting

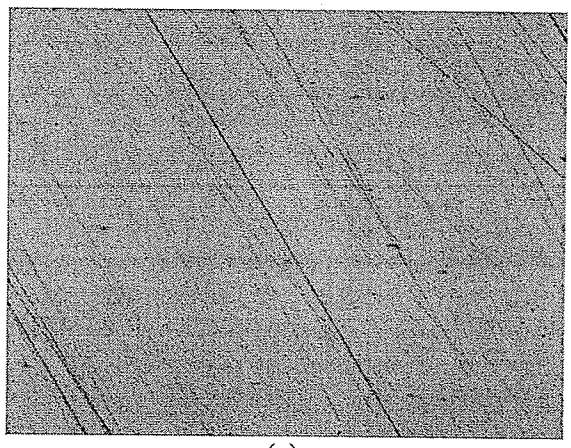

(a)

(b)

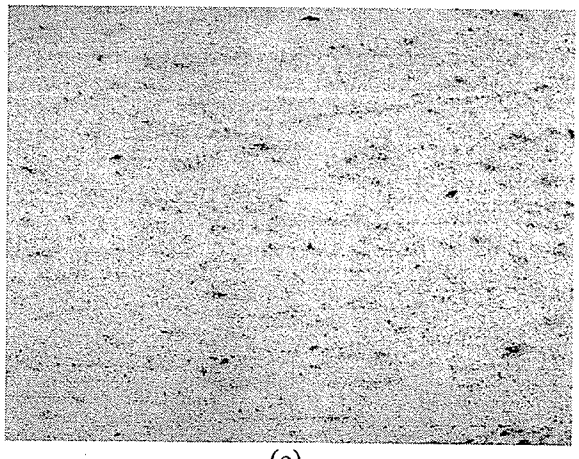

(c)

Fig. 3.12: Comparison between grinded and polished surface of copper sample at three different stages with minor pitting (x20 magnification): (a) grinding using 1200-mesh abrasive; (b) polishing using 6 micro-meter solution; (c) polishing using 1 micro-meter solution

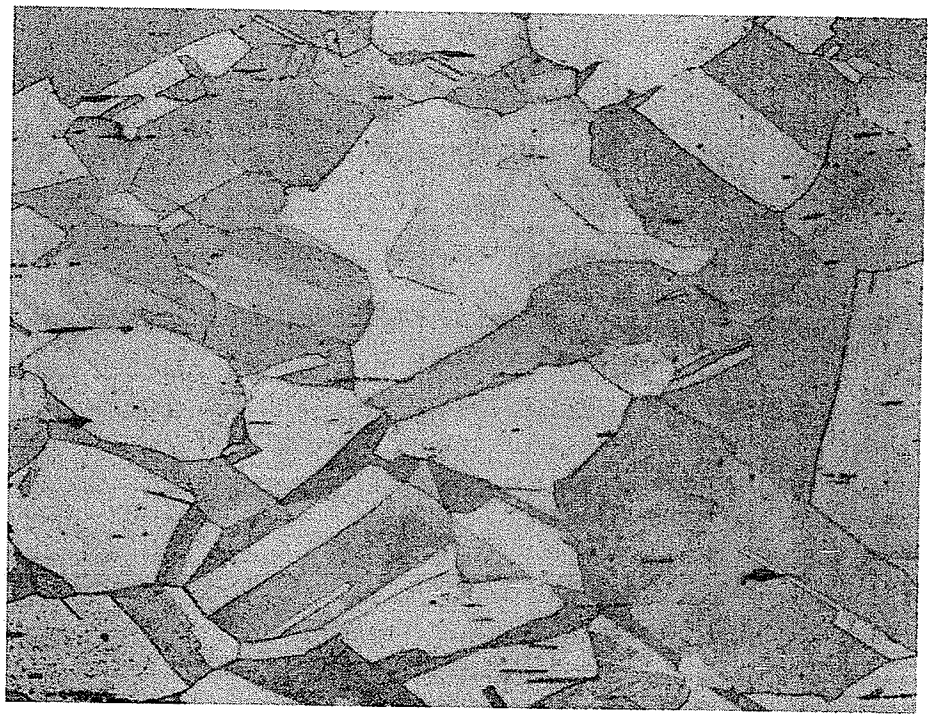

Fig. 3.13: Etched surface of Copper using Ferric Chloride solution (x20 magnifications). Note the present of numerous annealing twins which appear as lines within the grains.

3.4.2 Microstructure Analysis Methods

The prepared samples were examined using both optical and scanning electron microscopes. The light microscope has wide variety of use and one of the most important applications is the determination of the structural phases present and the physical make up of the bulk material such as: characteristics and phase distribution. However, there are two limitations associated with optical microscopy, namely resolution and depth of field. These are overcome by the use of Scanning Electron Microscope (SEM). The SEM shows images at much higher magnification, greater resolution and larger depth of field. In this study, Ziess optical microscope with the Clemex Vision Analyzer and JEOL JSM-5900 LV Scanning Electron Microscope with applied voltage of 20V, were used.

CHAPTER 4 – EXPERIMENTAL RESULTS & DISCUSSION

4.1 Experimental Results

4.1.1 Formation of Stress-Strain Curves

The signals from the two strain gauges are captured by the data acquisition system as voltage versus time data (Fig. 4.1). As shown on this figure, the input and output voltages gives incident, reflected and transmitted waves that are used to determine γ_I, γ_R and γ_T pulses. Using this initial data along with data from Table 1 in equations shown in Chapter 3, stress-strain curves as well as strain rates can be determined.

Once all the samples have been post processed and their corresponding curves generated, one curve most indicative from each of the four applied angles of twist is selected and compared throughout this research.

4.1.2 Dynamic Stress-Strain Curves

Under any type of applied load, either static or dynamic, the ductile material behaves in a way that follows a generally accepted form of stress-strain curve with some variations and can be divided into three sections such as: elastic deformation, adiabatic heating, and stress collapse as shown in Fig. 4.2. This figure is used to validate the appearance of the curves to follow in this thesis.

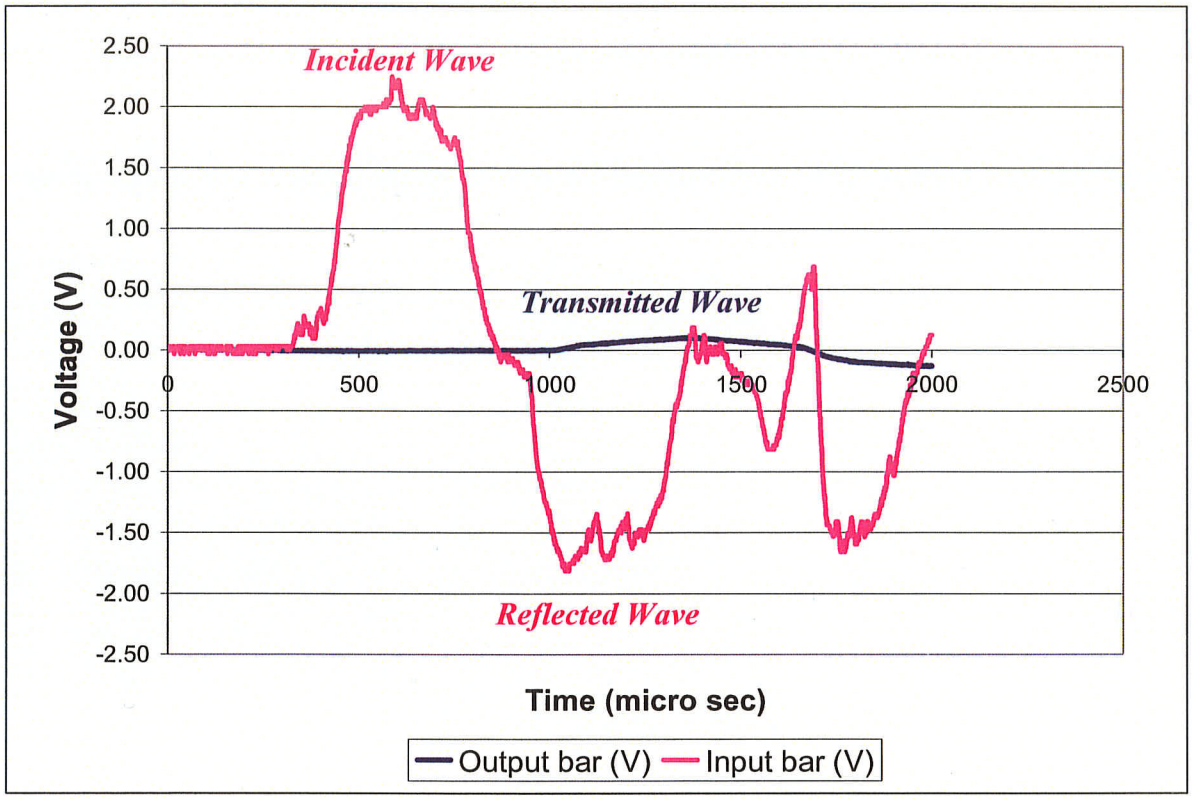

Fig. 4.1: Example of data acquired from the experiment to form a Voltage vs. Time graph

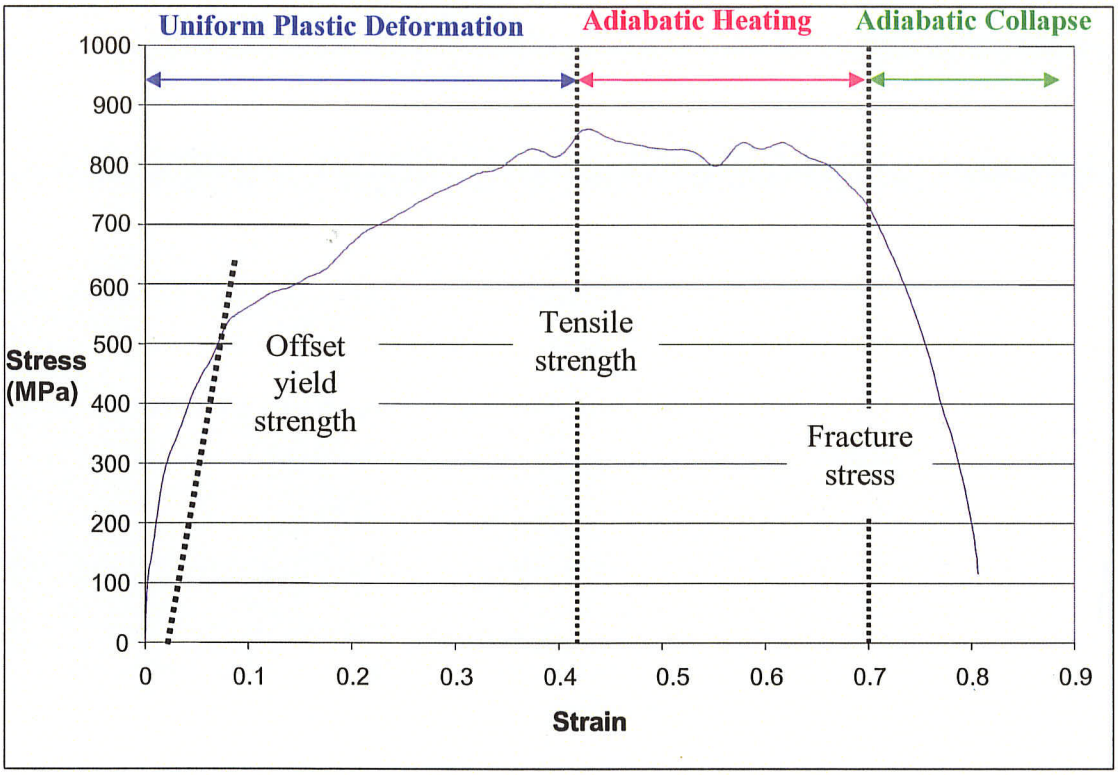

Fig. 4.2: Description of Different Sections of the Stress-Strain Curve

The first group of curves shown in Fig. 4.3 corresponds to the samples tested at 6° twist angle. The curve for sample 03 shows a slight yield drop near the yield point, but other than that, the rest are typical in their appearances and do not show a visible yield occurrence. Similar group curves are obtained for samples tested at 7°, 8° and 9° twist angles and their plots are shown in Fig. 4.4, 4.5 and 4.6 respectively. The summary of all the different values determined from these curves are presented in Table 2. In order to be able to visualize more readily the relative performance of each of the group types on the same scale, a composite figure consisting of one curve most indicative of each group is provided in Fig. 4.7, in order to represent the evolution of strain rate as increasing the angle of twist.

The resemblance between this work and the work of Schoenfeld and Wright [2] can easily be observed by comparing the figures obtained here with Fig. 2.3. Basically, in each case, the plastic deformation starts at the yield point and the process of strain hardening dominates this plastic deformation until a maximum flow stress is reached. It is beyond this point that thermal softening takes over and plays the major role in the deformation process due to the generation of adiabatic heating. As the strain increases, further decrease in flow stress occurs until the critical strain is reached, where a sharp drop indication of stress collapse is observed. The stress collapse occurs as a result of thermo-mechanical instability caused by thermal softening in the adiabatically heated region. Temperature increase up to the neighborhood of melting point of the deformed metal has been reported in the literature [45]. Chen *et al.* [45] reported an increase in temperature of above 1500°C in circular steel plate struck by a blunt projectile at very high velocity.

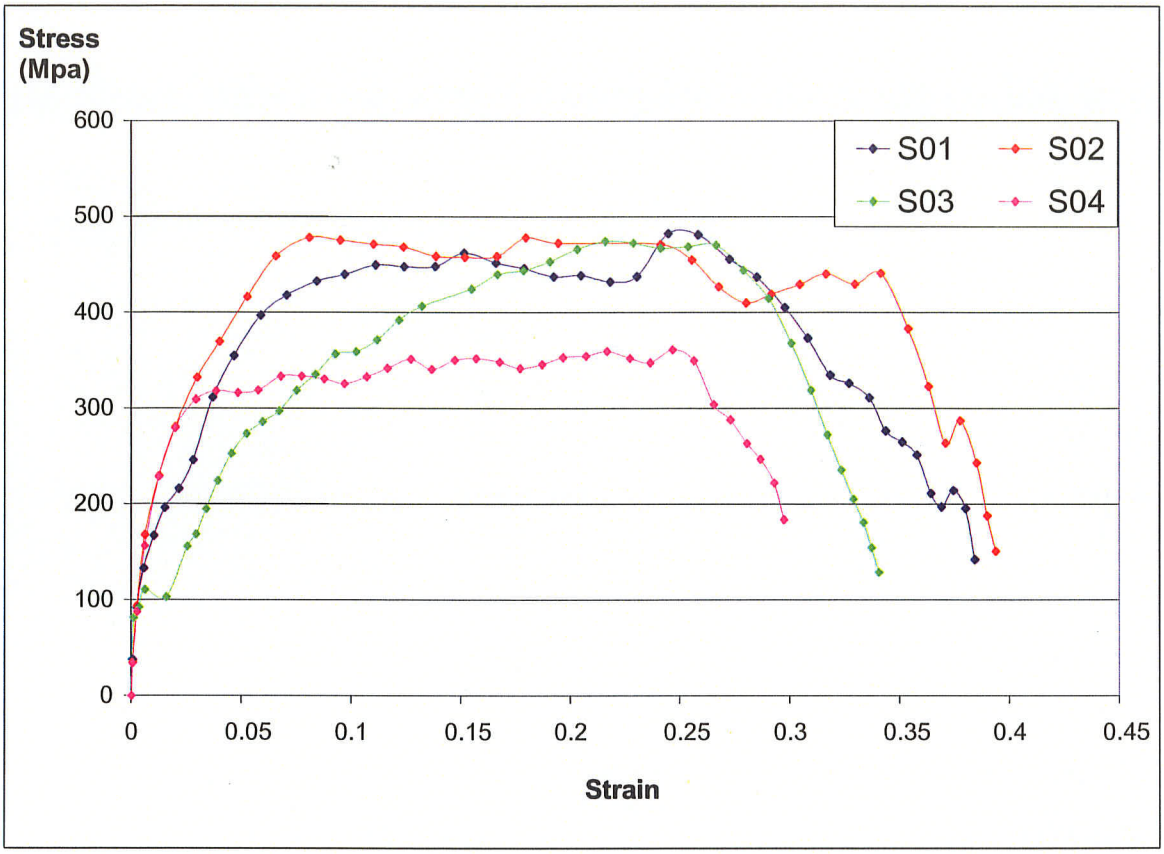

Fig. 4.3: Stress-Strain Curves for samples deformed at 6° twist angle

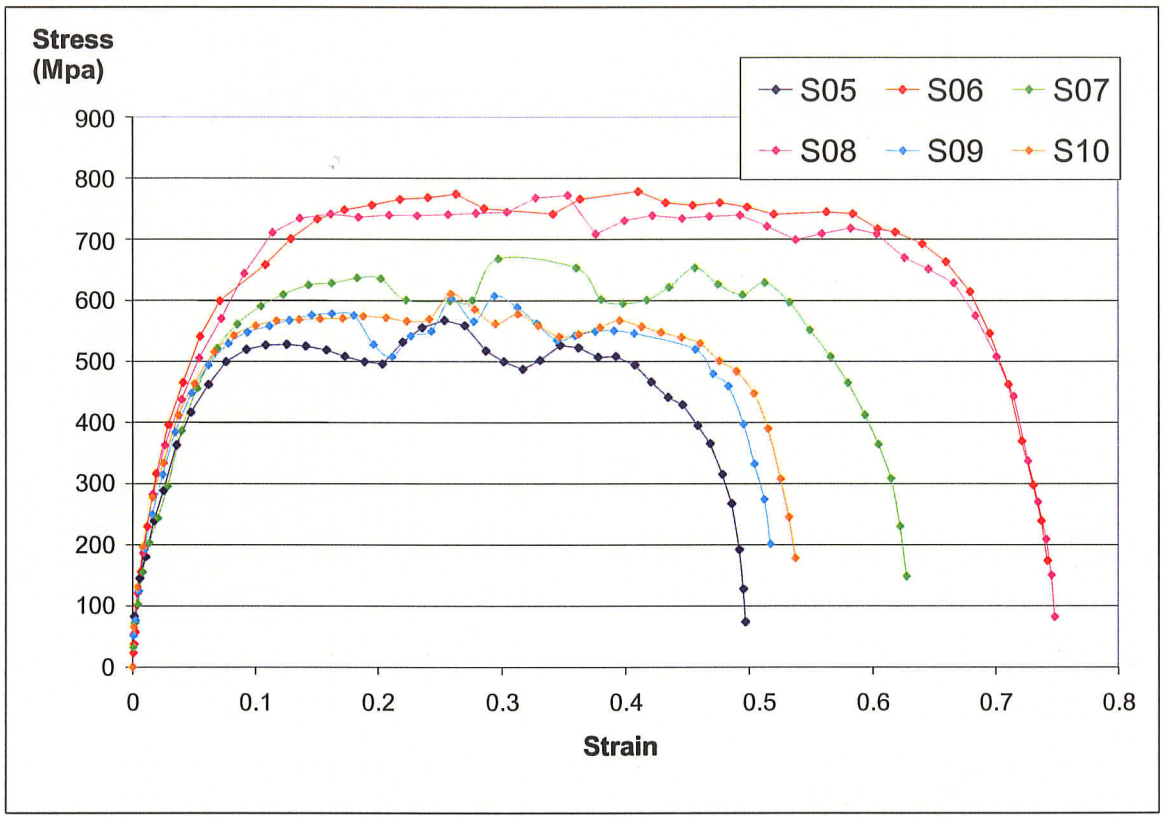

Fig. 4.4: Stress-Strain Curves for samples deformed at 7° twist angle

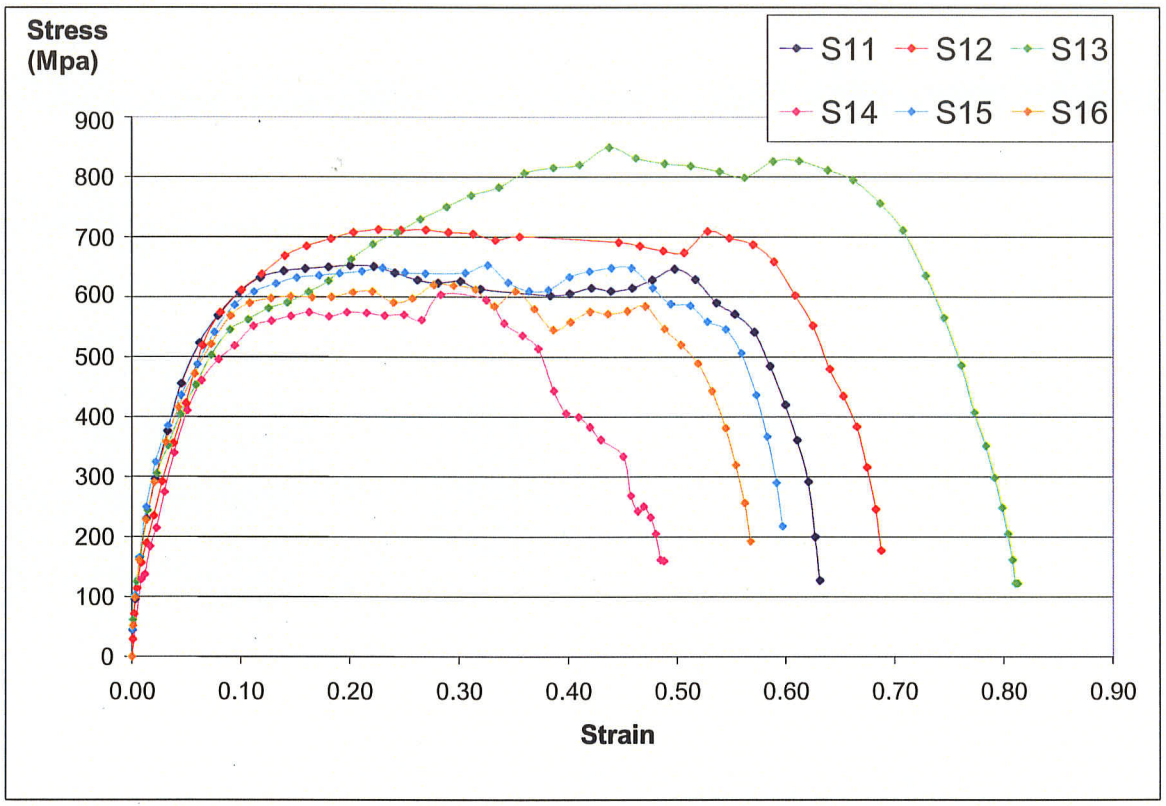

Fig. 4.5: Stress-Strain Curves for samples deformed at 8° twist angle

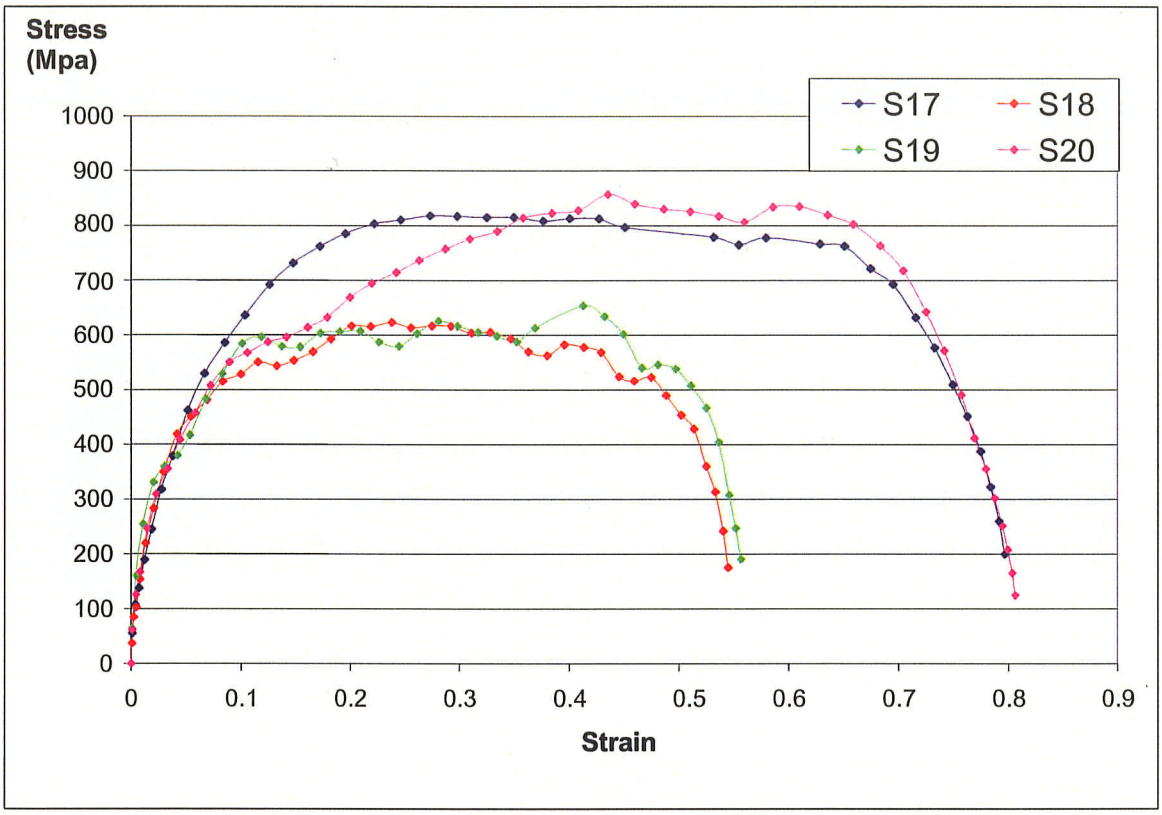

Fig. 4.6: Stress-Strain Curves for samples deformed at 9° twist angle

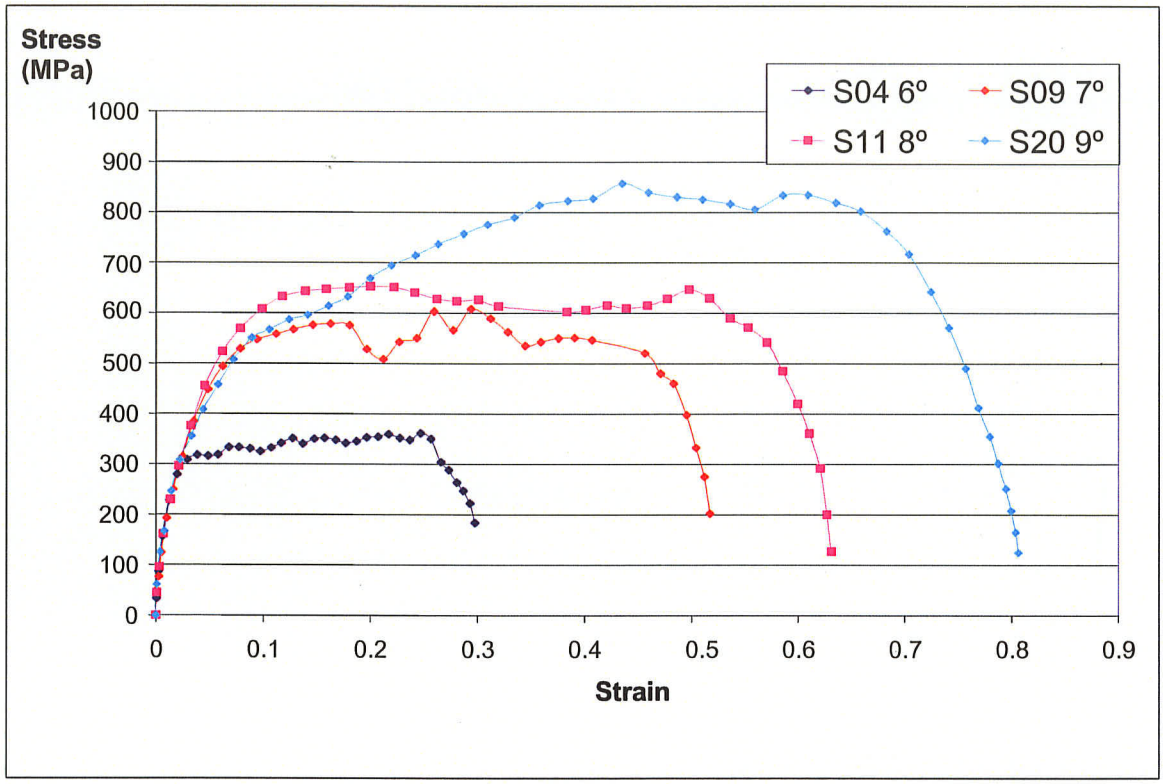

Fig. 4.7: Stress-Strain Curves of four selected samples tested at different twist angles

Table 2: Illustration of the Shear Stress vs. Shear Strain graphs for twenty specimens.

Angle of Twist (°) & Applied Torque (Nm)	*Sample #*	*Max. Strain Rate (1/s)*	*Max. Shear Stress (MPa)*	*Yield Point (MPa)*	*Strain at Yield*	*Adiabatic Heating Range (MPa)*	*Strain for AH*	*Collapse Stress (MPa)*	*Collapse Strain*	*Collapse Time (microsec)*
	1	684	486	246	0.030	437-486	0.255	437	0.285	142
6	2	729	478	230	0.015	383-478	0.335	383	0.350	158
265	3	641	474	111	0.005	415-474	0.285	415	0.290	195
	4	491	362	229	0.010	304-362	0.255	304	0.265	158
Average	——	636	450	204	0.015	385-450	0.283	385	0.298	163
	5	826	568	181	0.010	430-568	0.435	430	0.445	173
	6	1211	779	316	0.020	663-779	0.640	663	0.660	194
7	7	1036	668	204	0.015	597-668	0.515	597	0.530	179
310	8	1185	773	283	0.015	628-773	0.650	628	0.665	179
	9	886	608	194	0.010	460-608	0.475	460	0.485	185
	10	898	611	197	0.010	484-611	0.480	484	0.490	173
Average	——	1007	668	229	0.013	544-668	0.533	544	0.546	181
	11	1080	653	230	0.015	541-653	0.555	541	0.570	179
	12	1149	713	235	0.020	659-713	0.570	659	0.590	184
8	13	1255	850	306	0.020	711-850	0.685	711	0.705	194
354	14	866	604	184	0.015	443-604	0.370	443	0.385	147
	15	950	653	250	0.015	506-653	0.545	506	0.560	184
	16	916	620	228	0.015	489-620	0.505	489	0.520	179
Average	——	1036	682	239	0.017	558-682	0.538	558	0.555	178
	17	1361	818	246	0.020	693-818	0.675	693	0.695	184
9	18	886	623	220	0.015	523-623	0.460	523	0.475	179
398	19	1168	653	331	0.020	546-653	0.460	546	0.480	163
	20	1250	861	309	0.025	802-861	0.635	802	0.660	183
Average	——	1166	739	277	0.020	641-739	0.558	641	0.578	177

AH = Adiabatic Heating

The strain rate depends on the angular rotation (i.e. applied torsional loading) at the end of the incident bar which twist the test specimen when the load-release aluminum pin component of clamping mechanism fracture. The higher the twist angle, the greater is the amount of deformation at any given time and the greater is also the rate of deformation (Fig. 4.8). The average strain rate of the samples that were deformed by applying twist angles of 6°, 7°, 8° and 9° were calculated to be 636, 1007, 1036 and 1166 s^{-1} respectively. It is also clear in Fig. 4.8 and Table [2] that the yield and maximum flow stress as well as the maximum strain before stress collapse and adiabatic shearing also increase with the strain rate. Depending on the applied twist angle, the average critical strain and time for strain localization lies between 0.30 – 0.58 and 163 – 178 μs respectively.

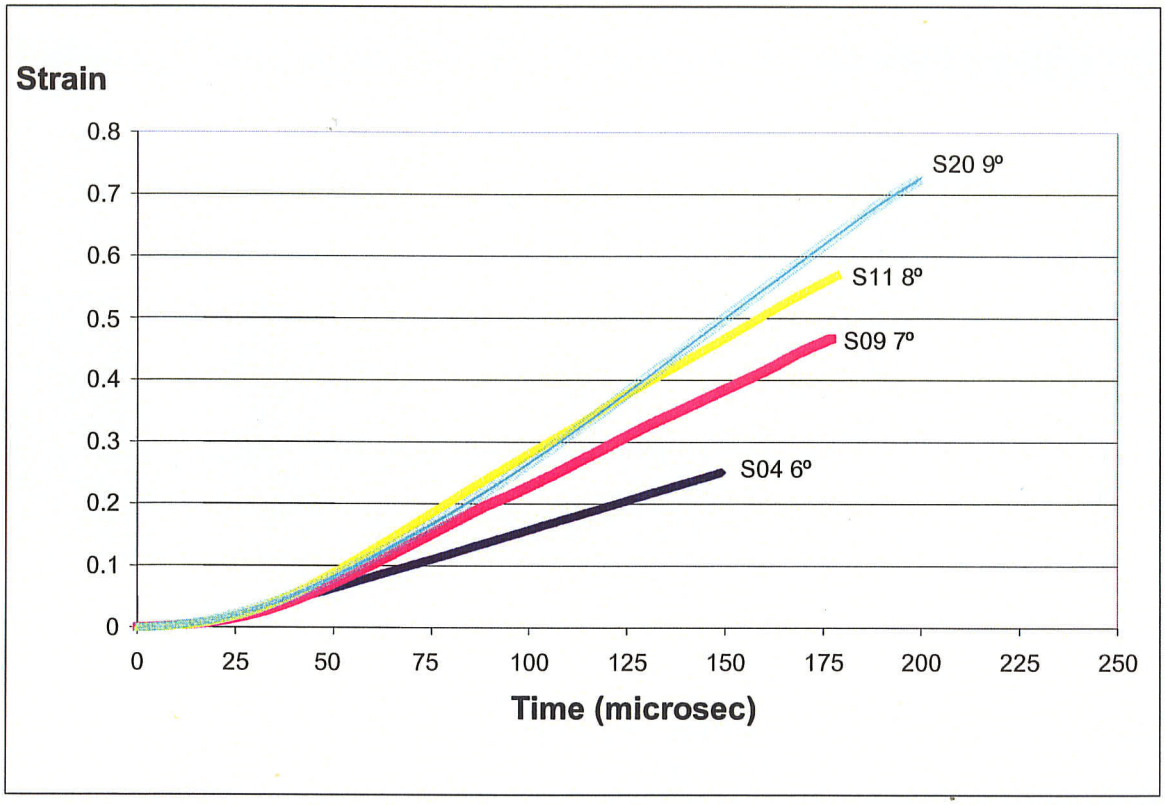

Fig. 4.8: Strain vs. Time Curves of four selected samples tested at different twist angles

The strain rate sensitivity of a material is mainly the slope of the natural logarithm of stress vs. natural logarithm of strain rate at a fixed shear strain [46]:

$$m = \left(\frac{\partial \log \tau}{\partial \log \dot{\gamma}} \right)_{\gamma}$$

According to the study by Mercier and Molinari [47] and Wright [48], materials with low strain rate sensitivity have higher instability and tendency to form adiabatic shear bands than the ones with high strain rate sensitivity.

Fig. 4.9 shows stress vs. logarithm of strain rate curves for copper at constant strain of 0.08, 0.15 and 0.25. The positive strain rate sensitivity of copper is clearly observable from this figure and it is also presented in Table [3]. Copper in general is considered to be a difficult material to experience strain localization due to its high ductility. However, the twinned structure and their influence on strain rate sensitivity cause the occurrence of plastic deformation inside the material. The underlying mechanism of these deformations will be examined in discussion section of this chapter.

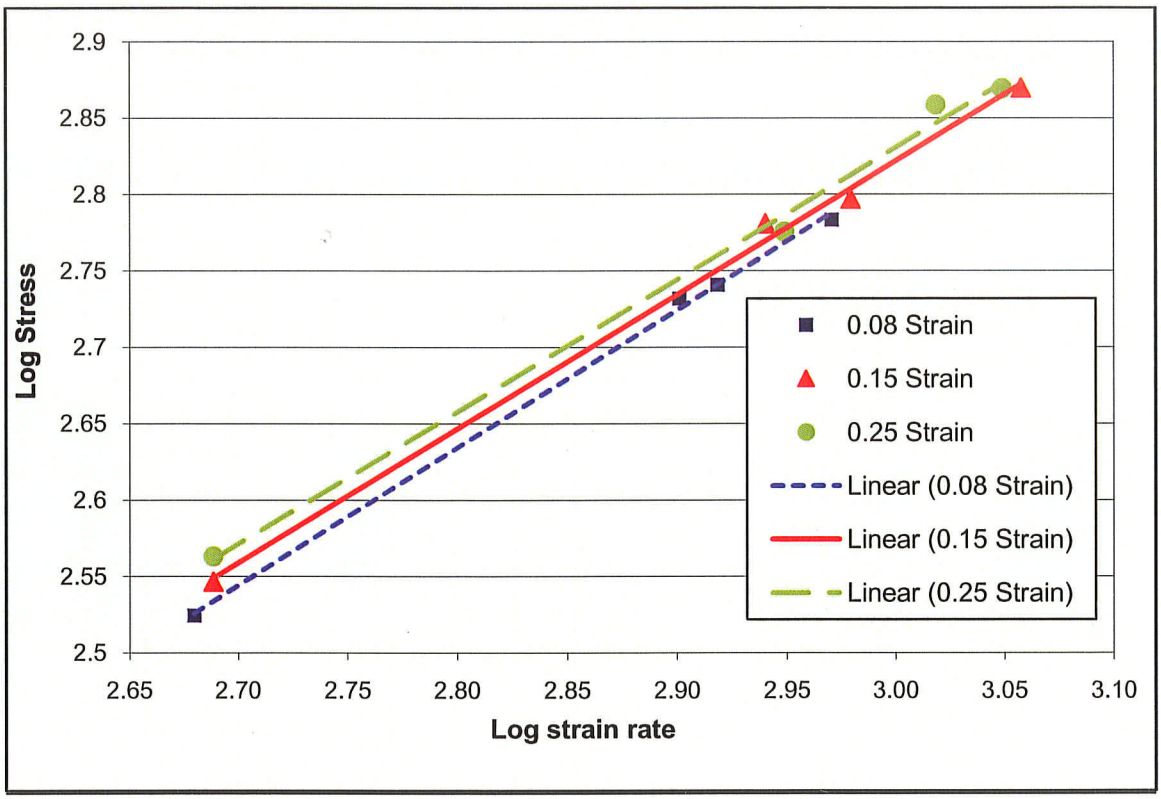

Fig. 4.9: Stress vs. Log strain-rate curves for the tested copper at fixed shear strain of 0.08, 0.15 and 0.25

Table 3: Strain rate sensitivities of investigated copper at shear strain of 0.08, 0.15 and 0.25

Material	*Strain rate sensitivity*		
	Strain = 0.08	***Strain = 0.15***	***Strain = 0.25***
Copper	0.889	0.876	0.864

4.1.3 Microstructural Evaluation of the Samples after Torsional Loading

Microstructural analysis was performed by sectioning the samples in longitudinal axis and preparing them as described in section 3.4. Optical microscopic examination of thin walled tube section of samples, show clearly the presence of grain boundaries, twins and some deformation zones that develop during machining or sectioning of samples (Fig. 4.10). However, when it comes to examining the detailed microstructure of the material and the presence of adiabatic shear bands, optical microscopy does not reveal this information due to its low resolution and depth of focus. Therefore, Scanning Electron Microscopy (SEM) is used for further examination of the tested samples.

The following SEM micrographs of several selected samples (Fig. 4.11 – 4.19) show the presence of adiabatic shear bands along with some deformation slip bands. These adiabatic shear bands are deformed type of shear bands; they have the same appearance as the bulk material but contain distorted grains. One can see from these figures that at lower strain rate, the adiabatic shear bands formation is relatively homogeneous compare to the ones formed at higher strain rate. Also, the visibility of these bands increases as the applied strain rate increases. The homogeneity in this study is noticeable as the shear bands are randomly spread across the thin-walled tube section.

In Fig. 4.13 and 4.17, the reorientation of the grains inside the shear band and the direction of flow pattern around the band are evident, which also follow the deformation mechanism introduced by Li *et al.* [14]. These viscous flow patterns become less visible with distance away from shear bands as a result of gradual reduction in thermal softening and plastic strain that occurs around the bands. Multiple shear bands were also observed

as shown in Fig. 4.15. Fully developed adiabatic shear bands across the thin-walled tube section are clearly evident even at much lower magnification (x300 and x100) in Fig. 4.18 and 4.19 respectively.

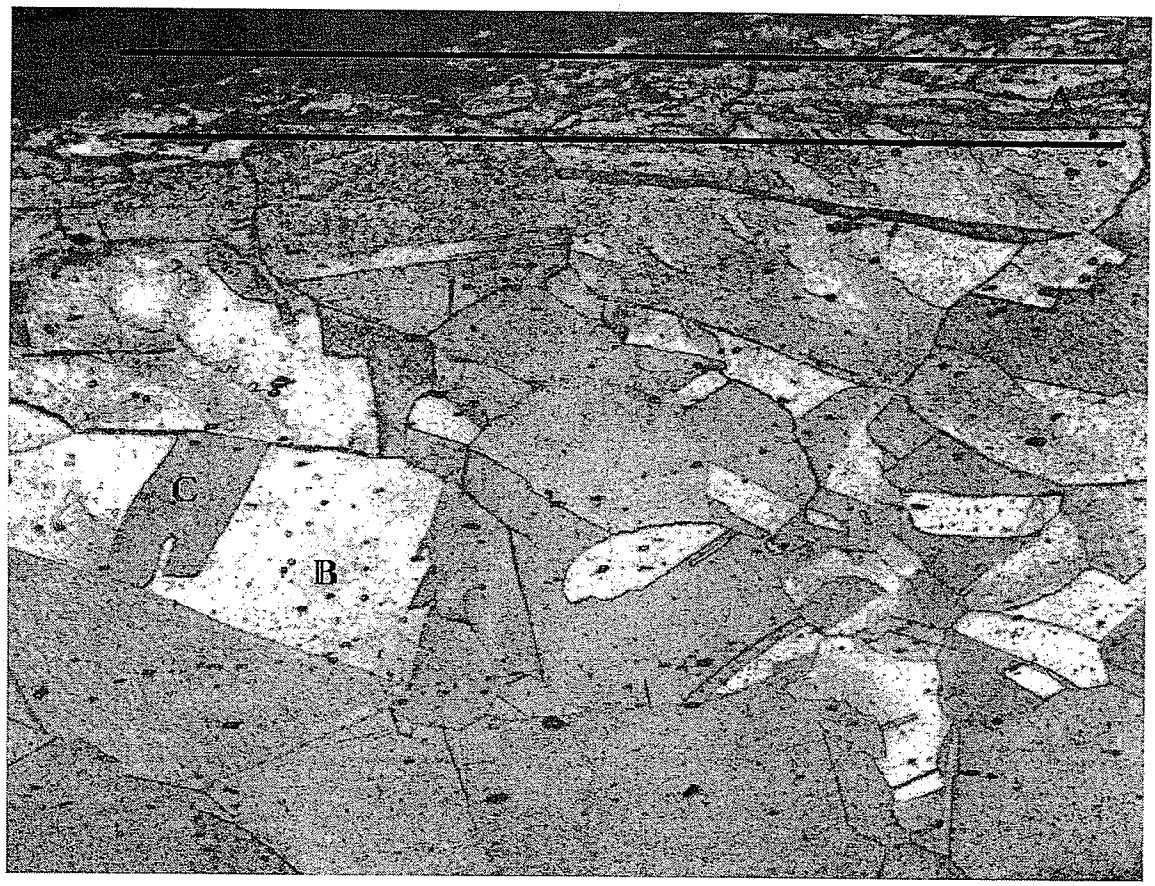

(x20 magnifications)

Fig. 4.10: Optical micrograph of a tested copper sample showing: A – deformation zone as a result of sectioning the sample, B – typical grain boundary and C – twins inside the grain.

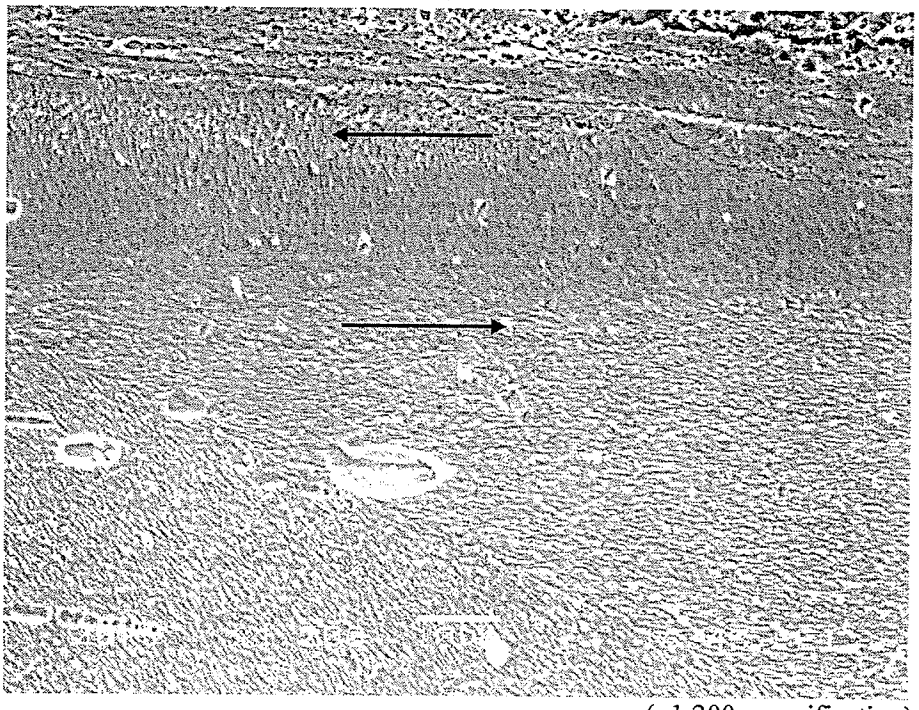

(x1,200 magnification)

Fig. 4.11: Typical sample tested at 6° twist angle (S04), strain rate of 491 s^{-1} and maximum strain of 0.3 showing a deformed shear band.

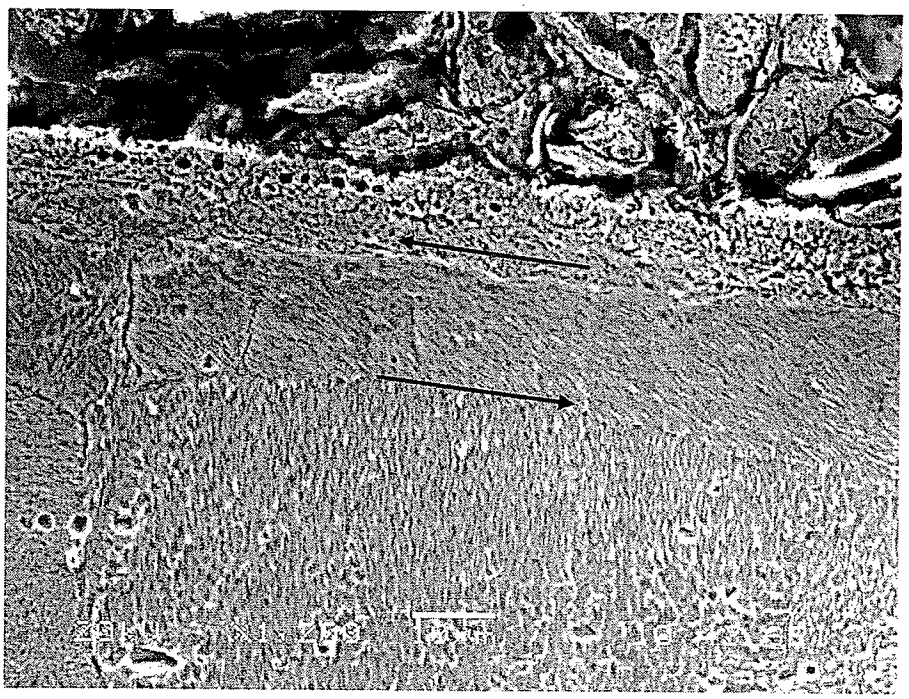

(x1,200 magnification)

Fig. 4.12: Typical sample tested at 6° twist angle (S01), strain rate of 684 s^{-1} and maximum strain of 0.4 showing a deformed shear band.

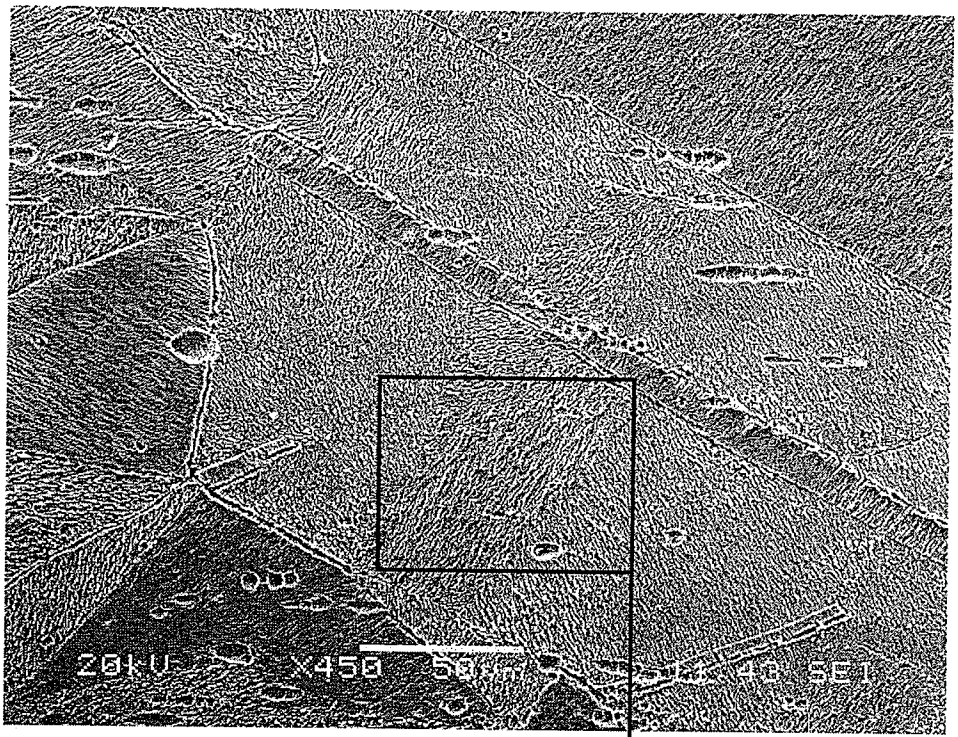

(x450 magnification)

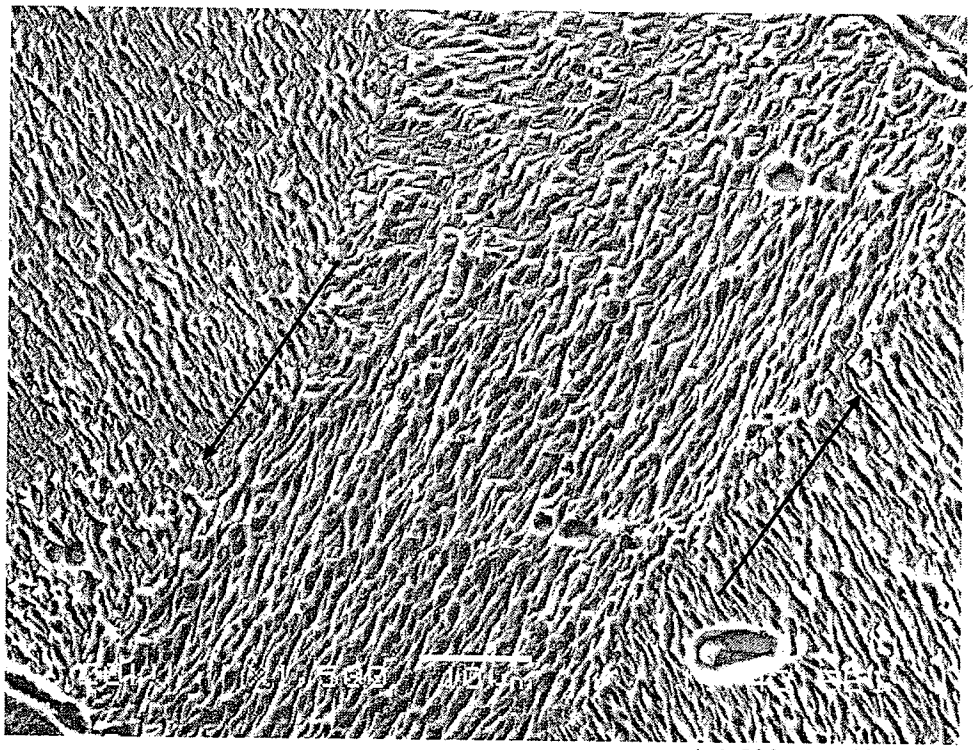

(x1,500 magnification)

Fig. 4.13: Typical sample tested at 7° twist angle (S09), strain rate of 886 s^{-1} and maximum strain of 0.52 showing the reorientation of the grains inside the shear band.

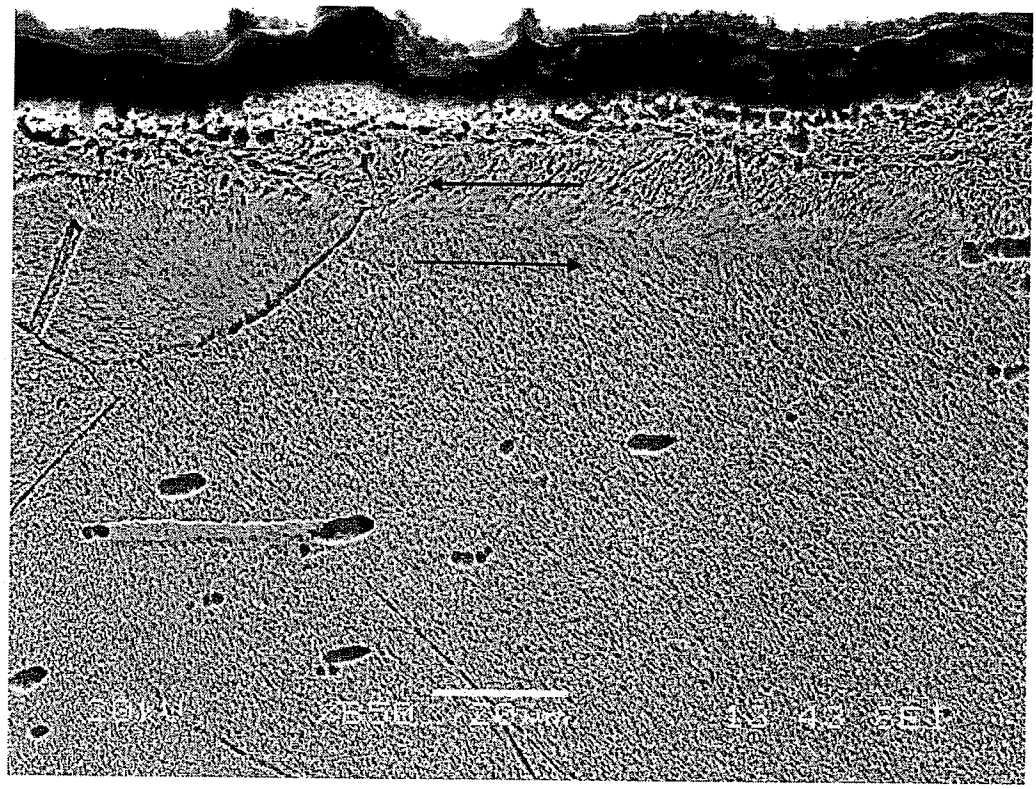

(x850 magnification)

Fig. 4.14: Typical sample (S09) showing a deformed shear band.

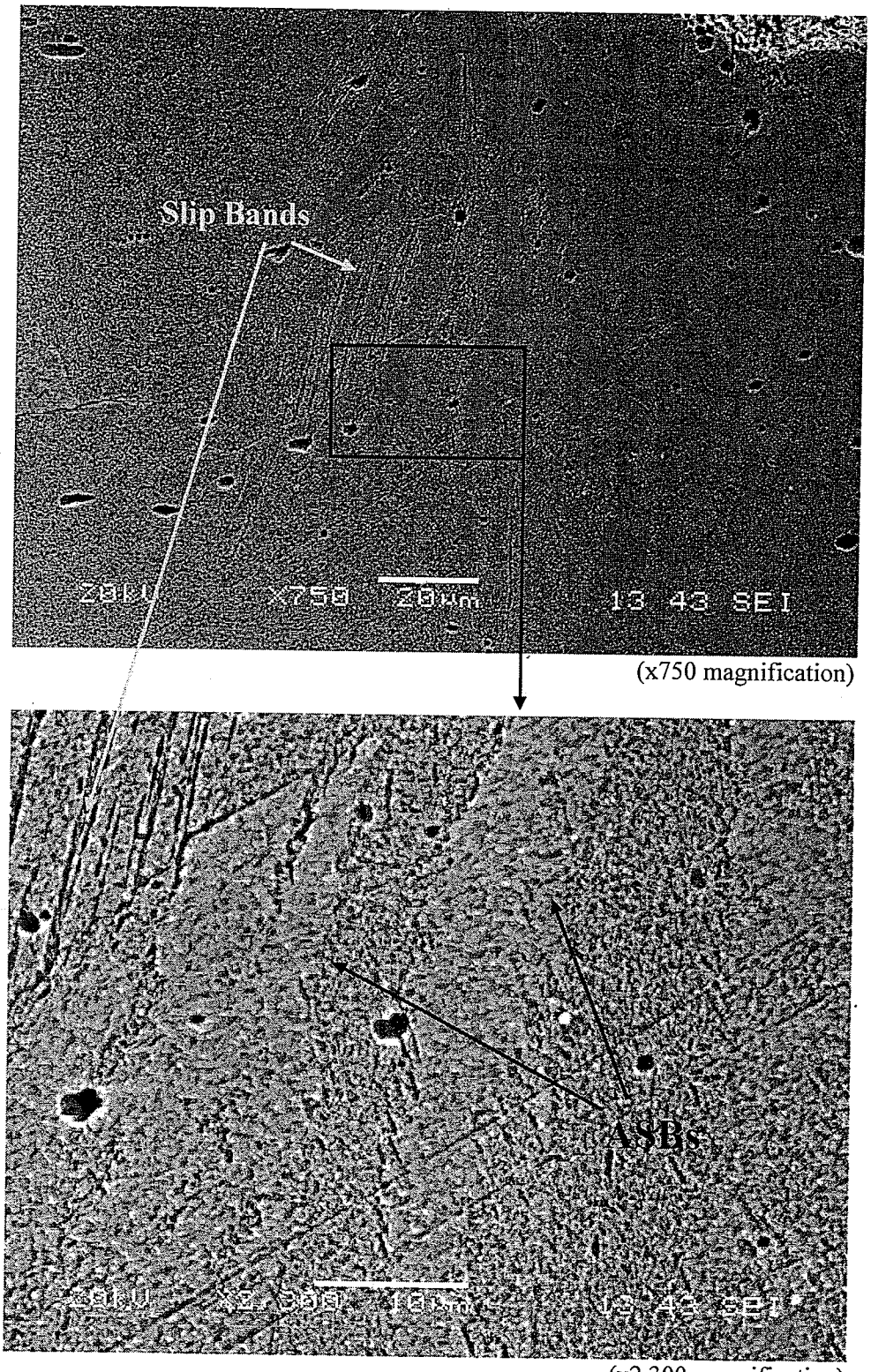

Fig. 4.15: Slip and multiple deformed shear bands in a typical sample tested at 8° twist angle (S11), strain rate of 1080 s^{-1}, maximum strain of 0.65.

(x450 magnification)

Fig. 4.16: Typical sample (S11) showing a deformed shear band.

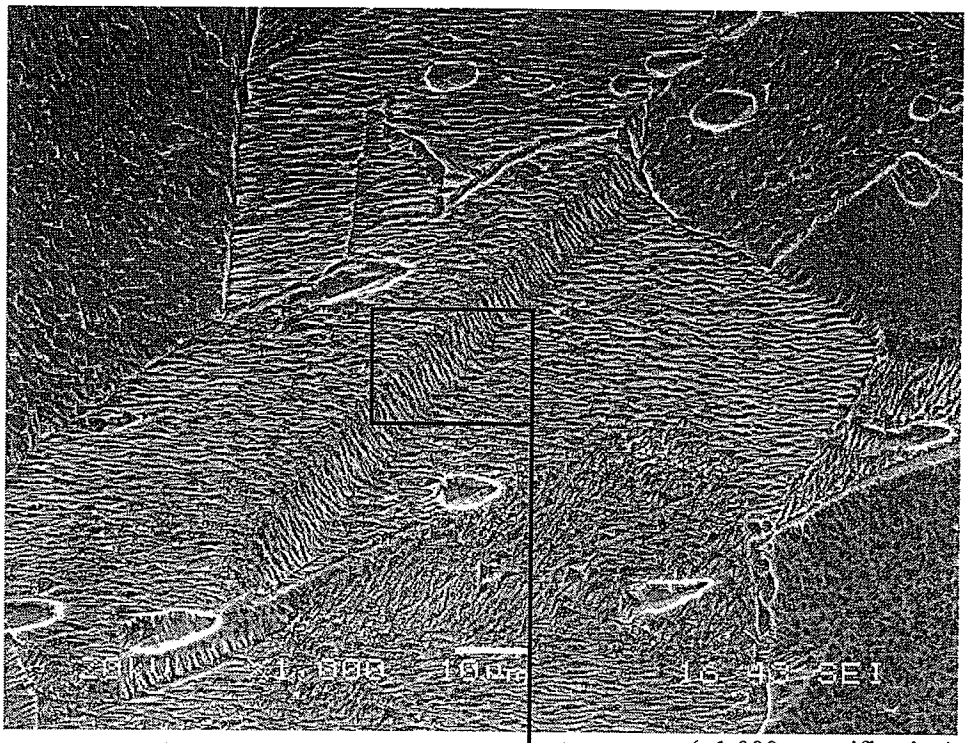

(x1,000 magnification)

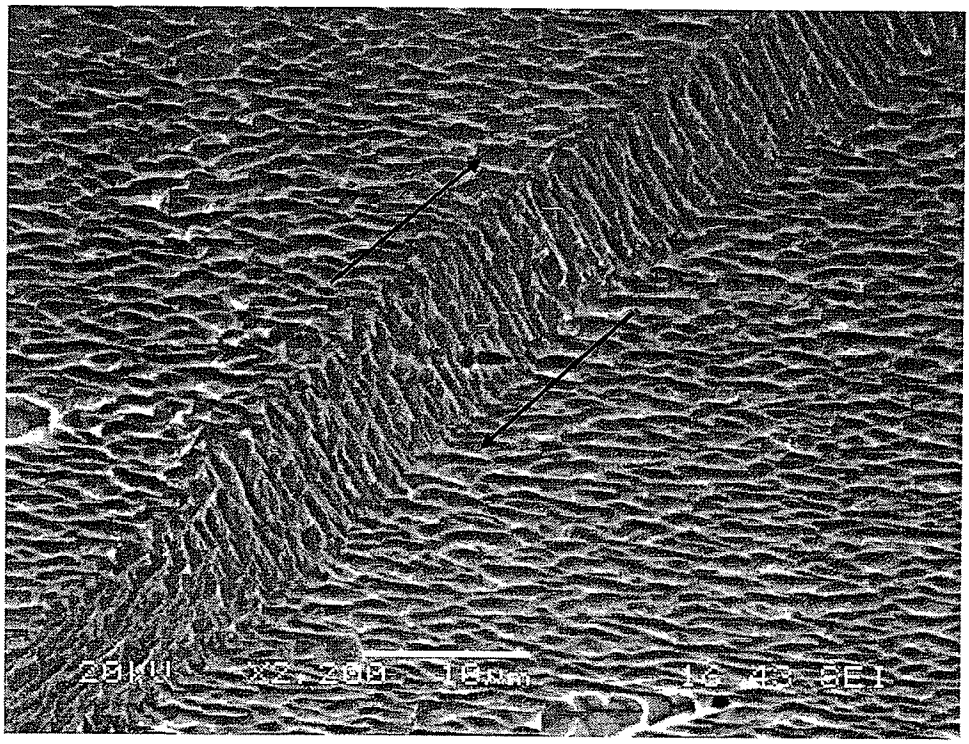

(x2,200 magnification)

Fig. 4.17: Typical sample tested at 9° twist angle (S20), strain rate of 1250 s^{-1} and maximum strain of 0.8 showing the reorientation of grains inside the shear band.

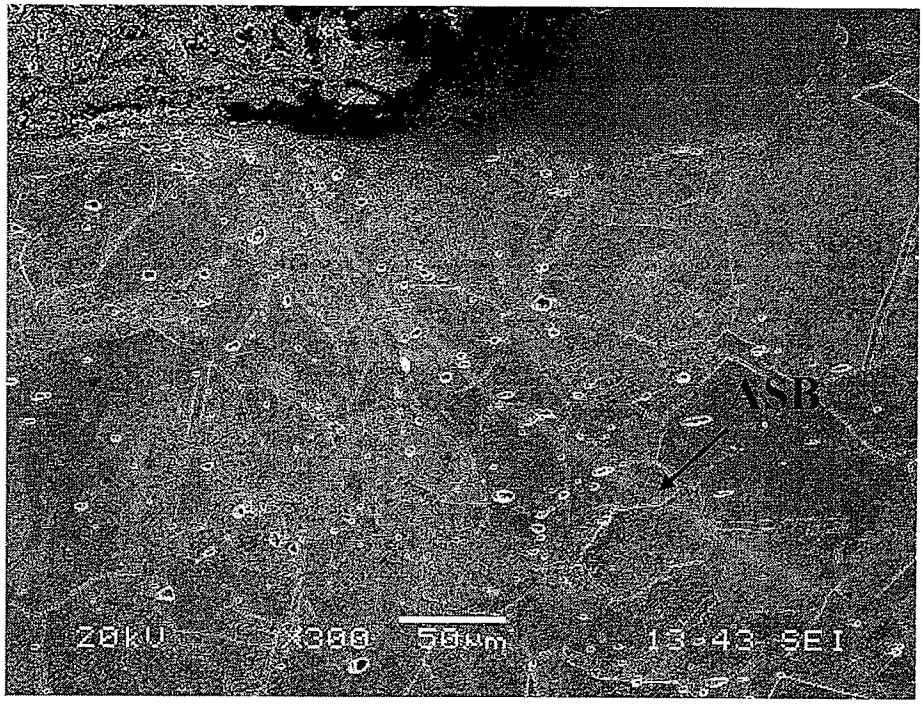

(x300 magnification)

Fig. 4.18: Typical sample (S20) revealing the fully developed adiabatic shear band.

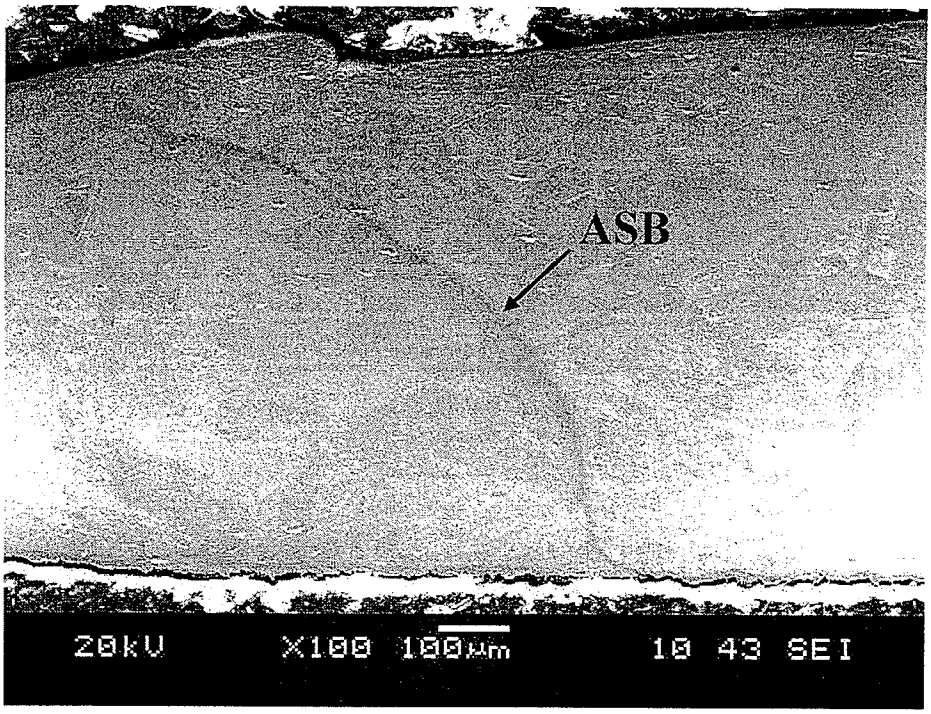

(x100 magnification)

Fig. 4.19: Typical sample tested at 9° twist angle (S19), strain rate of 1168 s^{-1} and maximum strain of 0.56 revealing the fully developed adiabatic shear band.

Finally, microstructural examination of the deformed copper sample (S20) reveals what seem to be fine equiaxed grains with an average diameter of 0.1-0.2 μm (Fig. 4.20). The sharp features of these grains are the result of dynamic recrystallization as it was investigated by Hines and Vecchio [20] and several other researchers. One question that always arises during high strain rate testing is whether the measured response represents the intrinsic material behavior or is affected by the adiabatic temperature rise during deformation. For this reason, the temperature rise within the shear band during deformation is obtained using the Zerilli and Armstrong constitutive equation for FCC materials [49] with the assumption introduced by Kapoor and Nemat-Nasser (1998) [10] that all the mechanical work gets converted into heat during adiabatic deformation process according to

$$\Delta T = \frac{\beta W_P}{\rho C_P} \tag{14}$$

where, β is the fraction of plastic work converted into heat, taken here to be 0.9, W_P is the plastic work, ρ and C_P are the density and heat capacity respectively. In this study, for stress level of sample (S20) σ = 858 MPa, ε = 0.44, ρ = 8960 kg/m^3 and C_P = 385 J/kg K, the temperature rise using equation 14 is found to be 100 K. This calculated temperature rise is less than 7.5% of the melting temperature of copper. Even though the mechanism of the recrystallization has not been addressed here, one can see the fact that this low temperature region cannot play a significant role in material recrystallization under high strain rate. Therefore, this suggests that a different mechanism maybe associated with the formation of these equiaxed grains within adiabatic shear bands.

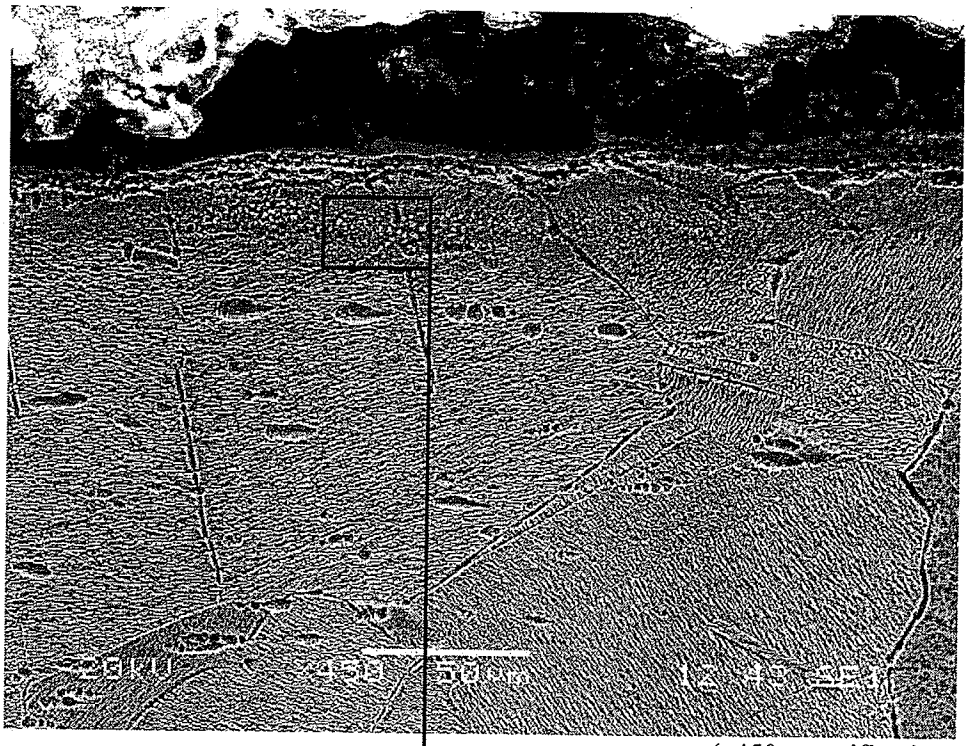

(x450 magnification)

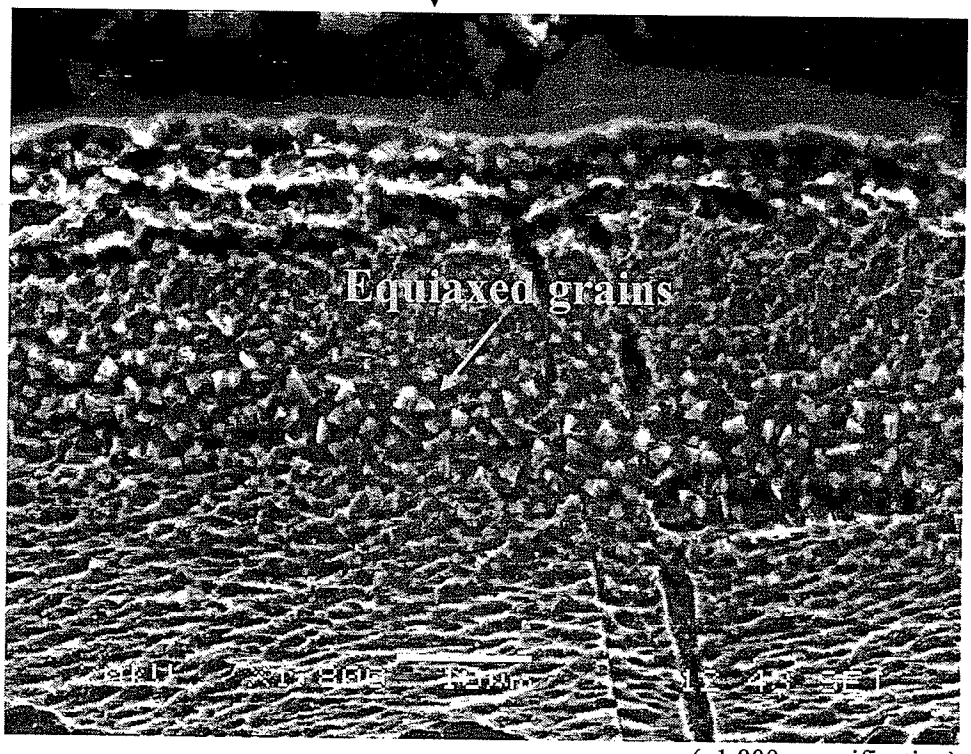

(x1,800 magnification)

Fig. 4.20: Equiaxed small grains (about one micron) that are characteristic of recrystallized material observed in a typical tested sample (S20).

4.2 Discussion of Results

The results presented in this thesis are centered on two main themes, namely the strain rate and microstructure dependency of adiabatic shear band formation in polycrystalline copper. Homogeneous distributions of plastic deformation and multiple adiabatic shear bands parallel to each other have been observed across thin-walled tube section of copper specimens. The presence of twins and slip bands cause segregations, which offer many initiation sites for adiabatic shear bands and enhance multiple adiabatic shear banding. This homogeneity feature of deformed shear bands can be considered being a result of random distribution of nucleation sites across the material.

Study by Stevenson *et al.* [50] also indicates that dislocation slip and twinning are the two possible deformation mechanisms in copper at high strain rates. These mechanisms are both stacking fault energy (SFE) and dislocation dependent. Basically, the lower the stacking fault energy in material, the higher is the twinning probability, which in turn increases the possibility of plastic deformation and formation of adiabatic shear bands. Among most FCC materials such as aluminum, which has a SFE of 166 mJ m^{-2} [40], copper has a lower SFE. It is due to this characteristic that makes the deformation more favorable in copper than in aluminum, even though, it was always previously thought that aluminum can flow easily than the copper because of its lower melting point [49]. Recent studies by Asaro and Suresh [51] suggest that the presence of twins emits dislocations to the vicinity of twin boundaries and create the shear band nucleation site similar to the dislocation pile-up mechanism described in Chapter 2.

It is also worth noting, from Fig. 4.21, the development of stepped twin boundaries as a result of high strain rate loading in the copper sample.

Examination of the stress-strain curves provided in section 4.1.2 of this chapter shows that the behavior of the samples upon yield varied from sample to sample in a similar manner, regardless of the applied twist angles. As it was mentioned earlier, only sample 03 experience a slight yield drop to relieve stress generated in the sample due to the interaction of dislocations, whereas the rest of the samples display continuous yielding that progress smoothly through the elastic-plastic section of curves. Discrepancy is also observed in the results obtained for the samples tested at 9° twist angle (Fig. 4.6). Two of the samples (S18 and S19) produce lower flow stress and strain than even the samples tested at lower strain rate, while the other two samples (S17 and S20) follow the more predictable pattern which is the increase in the flow stress and strain via the increase in the strain rate. This type of behavior can be considered to be the consequence of certain experimental error, such as slight slip in the incident bar after tightening the clamp may result in totally different applied torque than what it is desired.

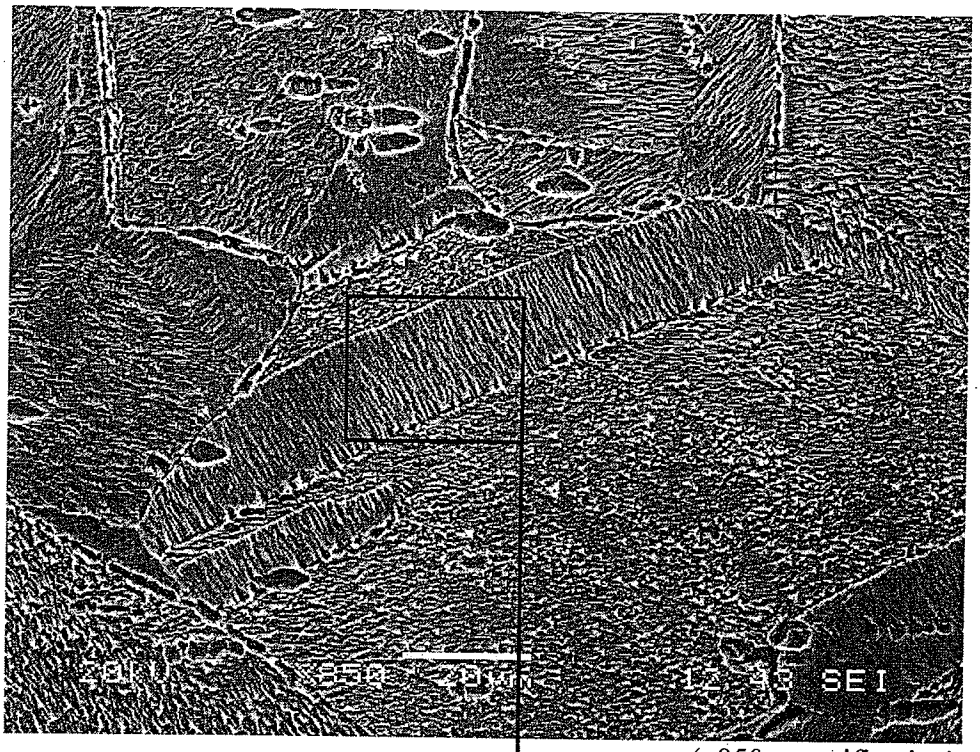

(x850 magnification)

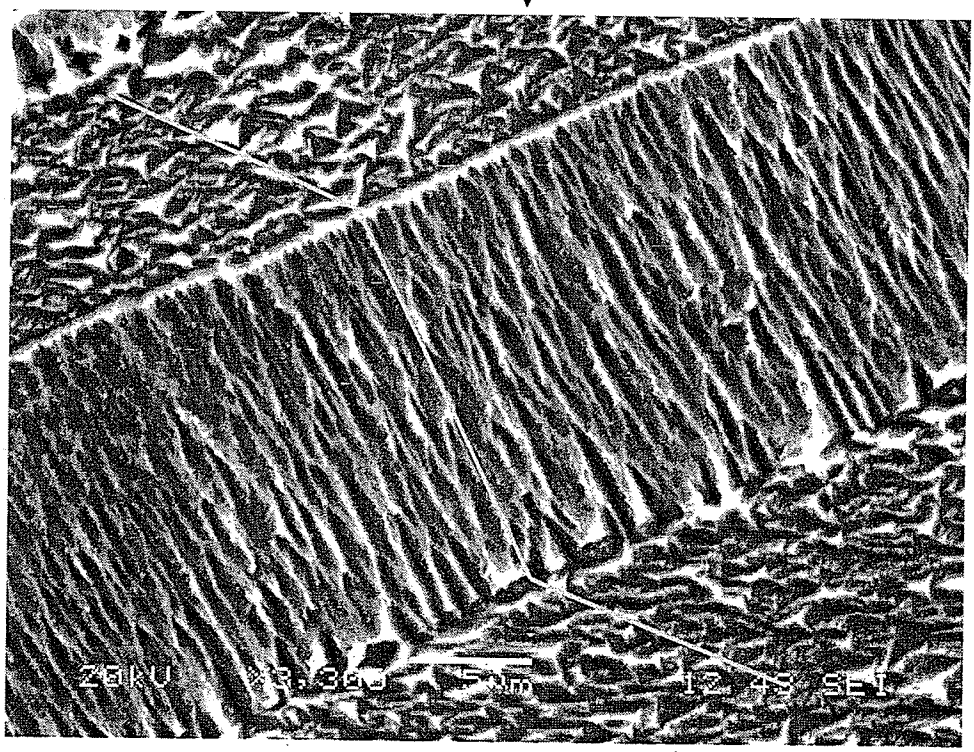

(x3,300 magnification)

Fig. 4.21: Typical SEM image of the stepped twin boundary in microstructure of a copper sample after torsional loading.

Examination of Table 2 and 3 along with the stress-strain curves reveal the positive strain rate sensitivity of copper. The results also clearly indicate that strain rate strongly affects the deformation of copper. The observed rate dependence of the flow stress and strain illustrate the increase of these properties of copper with increase in applied strain rate. The mechanism behind this increment in flow stress and strain following the change in strain rate can be described as a result of strain hardening due to dislocation multiplication, which tangle up and act as a barrier for dislocations motion. The dislocation tangles as well as inhomogeneous distribution of temperature inside the material during adiabatic heating, as it was studied by Schonefeld and Wright [2], are considered to be two of the perturbations that influence and enhance the chance of a speedy onset of stress collapse and occurrence of adiabatic shear bands can be seen in Table 2.

As previously mentioned in Chapter 2, there are two types of shear bands: deformed and white-etching (transformed) bands. Only deformed shear bands have been observed in copper samples. Three reasons are described here that support and explain the occurrence of only this type of deformation in copper: 1. the development of strong local stress concentration inside the material due to the high concentration of dislocations that are generated during high strain rate deformation, which increase the strength of the material, 2. the high ductility characteristic of copper in general as a result of ease of dislocations and twins mobility, and 3. the presence of only one phase in copper, which prevents it from undergoing any phase transformation as this is one of the characteristics of white-etching bands. These reasons to some extent also help the material to withstand the impact wear and cause delay in occurrence of any type of failure unless a critical

strain value is reached. In this research, none of the specimens failed, which leads to conclusion that a critical strain value for fracture is not reached; maybe because the maximum applied strain rate of 1361 s^{-1} was not high enough.

Detailed examinations of SEM micrographs of samples illustrate:

1. The resemblance between this work (Fig. 4.13 and 4.17) and the work of Li *et al.* [14] (Fig. 2.9) regarding the initiation of ASB as a result of the deviation of the persistent slip bands, which cause the increase in both dislocation density and the required stress to break through dislocation barriers.

2. The strong strain rate dependency of deformed shear bands formation in copper material and how the visibility and the length of shear bands increase with increasing applied strain rate. Comparing Fig. 4.18 and 4.19 with the rest of the SEM figures, illustrate the fact that by increasing applied strain rate, a small increase in strength and a significant loss in ductility occur in copper samples as a result of increase in dislocation interaction that link together to form cells. The continuous rotation of these individual cells relative to each other during deformation cause decrease in size of cells, which in turn increase a tendency of the microbands to extend from one grain boundary to another [52]. The propagation of the deformed shear bands across grain boundaries can also be described as a result of localized material softening and decrease in the flow stress required for dislocation motion due to the effect of adiabatic heating and temperature rise during high strain rate loading.

3. The formation of possibly equiaxed grains inside the shear band have been observed in this work (Fig. 4.20), which can consider to be the result of dynamic recrystallization. As it was also attained in the work of Hines and Vecchio [20], the recrystallization follows similar mechanism found by Meyers *et al.* [18] and Chichili D. R. *et al.* [19] which are described in Chapter 2.

It is also important to note that the present results are in agreement with most of the previous works. For example, the results obtained in this research regarding strain rate sensitivity are found to support both the work of Senseny *et al.* [53] in the sense that the positive strain rate sensitivity was found, as well as the work of Bitans and Whitton [54] that adiabatic shear bands are formed in copper; even though the work of these two authors are not in agreement with each other.

The present work also demonstrates the complex aspects of ASB formation mechanisms in copper than just the dislocation pile-up release that was found by Wright *et al.* [15]. This can be explained as the result of the large extended plastic deformation that was observed from the obtained dynamic stress-strain curves, which clearly indicate that the model of dislocation pile-up as well as the effect of thermal softening are not sufficient to play important roles in the mechanism behind the formation of ASBs in tested copper samples.

Based on the study by Bassim and Feng [24] regarding the localization of the shear strain at the most non-uniform part of the microstructure due to the presence of material and geometrical defects, one can expect the possibility of other models including such as that described by Li to take place in the formation of ASBs. The model of Li

shown in Fig. 2.9 is in agreement with experimental observations that indicate the occurrence of ASBs in copper. Such bands are more diffuse at low angle of twist (7°) than at higher angle of twist (9°). The resemblance between the experimental results and the model of Li which predicts ASB as intersection of slip bands forming dislocation structure, explain the occurrence of ASBs in commercially pure polycrystalline copper during plastic deformation.

CHAPTER 5: CONCLUDING REMARKS

The major objective of this research is to investigate the formation of adiabatic shear bands in pure copper and relate the results to the various material conditions and experimental variables used in this study. Adiabatic shear bands were formed by subjecting the copper samples to rapid deformation using Torsional Split Hopkinson bar. From the experimental results and discussion, the following conclusions may be drawn:

i. The constitutive behavior of copper was investigated in the range of strain rate from 491 – 1361 s^{-1} using Torsional Split Hopkinson bar.

ii. The adiabatic shear bands formed in the copper samples during the high strain rate torsional loading are of the deformed type.

iii. The shear band deformation in tested copper sample is both strain rate and microstructural dependent. The higher the strain rate, the shorter is the time for the initiation of stress collapse and strain localization.

iv. Homogenous distribution and multiple adiabatic shear bands have been observed across thin-walled tube sections of specimens as a result of homogenously distribution of twins, which may act as initiation sites for ASBs formation.

v. The positive strain rate sensitivity of copper is clearly observed in this research. The continuous decrease in strain rate sensitivity values as a result of increasing applied strain rate by increasing the angle of twist is clear in Table [3].

vi. It is observed that copper undergoes significant plastic deformation at high strain rates and that ASBs may occur in the ascending part of the stress strain curve which the specimen is undergoing strain hardening.

vii. The results confirm the earlier model of Li which attributes ASBs to intersection of slip bands and formation of dislocation networks in copper, as opposed to the pile-up model commonly cited.

REFERENCES

[1] Al-Ameeri S., *The effect of heat treatment on the adiabatic shear bands in AISI 4340 steel at high strain rate*, University of Manitoba, (M. Sc. Thesis) 2005

[2] Schoenfeld S. E., Wright T. W., *A failure criterion based on material instability*, International Journal of Solids and Structures, Vol. 40 (2003) 3021-3037

[3] Zener C., Hollomon J. H., *Effect of strain rate upon plastic flow of steel*, Journal of Applied Physics, Vol. 15 (1944) 22-32

[4] Bai Y., Dodd B., *Adiabatic Shear Localization: Occurrence, Theories and Applications*, 1st Edition (1992)

[5] Wright P. K., *Metallurgical effects at high strain rates in the secondary shear zone of the machining operation*, edited by Rohde, Butcher, Holland and Karnes, Plenum Press (1973) 547-558

[6] Marchand A. and Duffy J., *An Experimental Study of the Formation Process of Adiabatic Shear Bands in a Structural Steel,* Journal of Mechanics and Physics of Solids, Vol. 36 (1988) 251-283

[7] Odeshi A. G., Bassim M. N., Al-Ameeri S., Li Q., *Dynamic Shear Band Propagation and Failure in AISI 4340 Steel,* Journal of Material Processing Technology, Vol. 169 (2005) 150-155

[8] Rogers H.C., *Adiabatic Plastic Deformation,* Annual Review of Materials Science, Vol. 9 (1979) 283-311

[9] Timothy S.P., *The Structure of Adiabatic Shear Bands in Metals: A Critical Review*, Acta Metallurgica, Vol. 35, No. 2 (1987) p 301-306

[10] Kapoor R., Nemat-Nasser S., *Determination of temperature rise during high strain rate deformation*, Mechanics of Materials, Vol. 27 (1998) 1-12

[11] Zhang B., Li Y., Shen W., Wang Y., Tang X., Wang X., *A Study on the Behavior of Adiabatic Shear Bands in Impact Wear,* Wear 198 (1996) 287-292

[12] Leech P.W., (1985) *Metallurgical Transactions,* 16A, 1900-103
http://www.mechse.uiuc.edu/research/gioia/Shear/profileShear.html

[13] Li G. A., Zhen L., Lin C., Gao R. S., Tan X., Xu C. Y., *Deformation Localization and Recrystallization in TC4 Alloy under Impact Condition,* Materials Science and Engineering, A 395 (2005) 98-101

[14] Li S. X., Yang R. Q., Li J. W. and Zhang Z. F., *Shear Localization in Dynamic Deformation of Copper Single Crystals,* Philosophical Magazine, Vol. 86, No. 36, 21 (2006) 5769-5786

[15] Nesterenko V. F., Meyers M. A., Wright T. W., *Self Organization in the Initiation of Adiabatic Shear Bands,* Acta Materialia, Vol. 46 (1998) 327-340

[16] Peirce D., Asaro R. J., Needleman A., *Material Rate Dependence and Localized Deformation in Crystalline Solids,* Acta Metallurgica, Vol. 31 (1984) 1951-1976

[17] Anand L., Kalinidi S. R., *The process of Shear Band Formation in Plane Strain Compression of FCC Metals: Effects of Crystallographic Texture,* Mechanics of Materials, Vol. 17 (1994) 223-243

[18] Mishra A., Richard V., Gregori F., Asaro R. J., Meyers M. A., *Microstructural evolution in copper processed by severe plastic deformation*, Journal of Material Science and Engineering, A 410-411 (2005) 290-298

[19] Chichili D. R., Ramesh K. T., Hemker K. J., *Adiabatic shear localization in α-titanium: experiments, modeling and microstructural evolution*, Journal of the Mechanics and Physics of Solids, Vol. 52 (2004) 1889-1909

[20] Hines J. A. and Vecchio K. S., *Recrystallization Kinetics within Adiabatic Shear Bands*, Acta Metallurgica, Vol. 45 (1997) 635-649

[21] Bassim M. N., *Study of the Formation of Adiabatic Shear Bands in Steels,* Journal of Materials Processing Technology, Vol. 119 (2001) 234-236

[22] Zhang B., Shen W., Liu Y. J., Zhang R., *Some Factors Influencing Adiabatic shear banding in impact wear*, Wear 214 (1998) 259-263

[23] Cepus E., *Evolution of Adiabatic Shear Bands in High Strength Steels at High Shear-Strain Rates*, University of Manitoba, (M. Sc. Thesis) 1995

[24] Feng H. and Bassim M. N., *Finite Element Modeling of the Formation of Adiabatic Shear Bands in AISI 4340 Steel,* Material Science and Engineering, A266 (1999) 255-260

[25] Schmidt C. G., Caligiuri R. D., Giovanola J. H. and Erlich D. C., *Effect of Grain Size on High Strain Rate Deformation of Copper,* Metallurgical Transactions, Vol. 22A (1991) 2349-2357

[26] Gorham D. A., *The Effect of Specimen Dimensions on High Strain Rate Compression Measurements of Copper,* Applied Physics, Vol. 24 (1991) 1489-1492

[27] Xue Q., Meyers M. A., Nesterenko V. F., *Self Organisation of Shear Bands in Titanium and Ti-6Al-4V Alloy,* Acta Materialia, Vol. 50 (2002) 575-596

[28] Campagne L., Daridon L. and Ahzi S., *A Physically Based Model for Dynamic Failure in Ductile Metals,* Mechanics of Materials, Vol. 37 (2005) 869-886

[29] Stroh N., *A Theory of the Fracture of Metals,* Advanced Physics, Vol. 6 (1957) 418-465

[30] Curran D. R., Seaman L., Shockey D. A., *Dynamic Failure of Solids,* Physics Reports, Vol. 147, No. 5-6 (1987) 253-388

[31] Meyers M. A., *Dynamic Failure: Mechanical and Microstructural Aspects,* Journal De Physique IV, Vol. 4 (1994)

[32] Hopkinson J., *Original Paper by J. Hopkinson,* B. Hopkinson, Ed., Cambridge: At the University Press, Vol. 2 (1901) 316-324

[33] Metals Handbook Ninth Edition, *Mechanical Testing,* American Society for Metals, Vol. 8 (1985) 198-228

[34] Davies R. M., *A Critical Study of the Hopkinson Pressure Bar,* Royal Society of London - Philosophical Transactions Series A, Vol. 240 (1948) 375-457

[35] Kolsky H., *An Investigation of the Mechanical Properties of Materials at Very High Rates of Loading,* Proceedings Physics Society, Vol. 62 (1949) 676-700

[36] Lindholm U. S. and Yeakely L. M., *High Strain Rate Testing: Tension and Compression,* Experimental Mechanics, Vol. 8 (1968) 1-9

[37] Staab G. H. and Gilat A., *A Direct-Tension Split Hopkinson Bar for High Strain-Rate Testing,* Experimental Mechanics, Vol. 31 (1991) 232-235

[38] Duffy J., Campbell J. D., and Hawley R. H., *On the Use of a Torsional Split Hopkinson Bar to Study Rate Effect in 1100-O Aluminum,* Journal of Applied Mechanics (Trans. ASME), Vol. 38 (1971) 83-91

[39] ASM Handbook, *Mechanical Testing and Evaluation,* American Society for Metals International, Vol. 8 (2000) 505-515

[40] Varma S. K., Caballero V., Ponce J., De la Cruz A., Salas D., *The Effect of Stacking Fault Energy on the Microstructural Development During Room Temperature Wire Drawing in Cu, Al and Their dilute Alloys,* Journal of Materials Science, Vol. 31 (1996) 5623-5630

[41] Tanner A. B. and McDowell D. L., *Deformation, Temperature and Strain Rate Sequence Experiments on OFHC Cu,* International Journal of Plasticity, Vol. 15 (1999) 375-399

[42] Sribniak A., *High Strain Rate Testing Using the Torsional Split Hopkinson Bar,* University of Manitoba, (B. Sc. Thesis) 2005

[43] Bassim M. N., *High Strain Rate Evaluation of Armor Materials,* University of Manitoba, 2007

[44] Fullingham P. J., Leary H. J. and Turner L. E., *Electron Microscopy and Structure of Metals,* (ed. G. Thomas), University of California Press, Berkely (1972) 163-172

[45] Chen X. W., Li Q. M. and Fan S. C., *Initiation of Adiabatic Shear Failure in a Clamped Circular Plate Struck by a Blunt Projectile,* International Journal of Impact Engineering, Vol. 31 (2005) 877-893

[46] Shen Y. F., Lu L., Dao M. and Suresh S., *Strain Rate Sensitivity of Cu With Nanoscale Twins*, Scripta Materialia, Vol. 55 (2006) 319-322

[47] Mercier S. and Molinari A., *Role of Rate Effects and of Thermomechanical Coupling in Shear Localization*, Transactions of the ASME, Vol. 119, No. 4 (1997) 322-331

[48] Wright T. W., *On the Speed of an Unconstrained Shear Band in a Perfectly Plastic Material,* International Journal of Solid and Structures, Vol. 40 (2003) 871-879

[49] Zerilli F. J. and Armstrong R. W., *Dislocation-Mechanics-Based Constitutive Relations for Material Dynamics Calculations,* Journal of Applied Physics, Vol. 61 (1987) 1816-1825

[50] Stevenson M. E., Jones S. E. and Bradt R. C., *The High Strain Rate Dynamic Stress-Strain Curve for OFHC Copper,* Materials Science Research International, Vol. 9 (2003) 187-195

[51] Asaro R. J. and Suresh S., *Mechanistic Models for the Activation Volume and Rate Sensitivity in Metals with Nanocrystalline Grains and Nano-scale Twins*, Acta Materialia, Vol. 53 (2005) 3369-3382

[52] Shankaranarayan H. and Varma S. K., *Strain-rate and Grain-size Effect on Substructures and Mechanical Properties in OFHC Copper during Tension*, Journal of Materials Science, Vol. 30 (1995) 3576-3586

[53] Senseny P. E., Richman M. H., and Duffy J., *The Influence of Annealing Temperature on the Strain Rate Sensitivity of Copper in Torsion*, Journal of Applied Mechanics, Vol. 42 (1975) 245-246

[54] Bitans K., and Whitton P. W., *Stress-Strain Curves for Oxygen Free High Conductivity Copper at Shear Strain Rates of Up to 10^3 s^{-1}*, Proceedings of the Institution of Mechanical Engineers, Vol. 185 (1970-1971) 1149